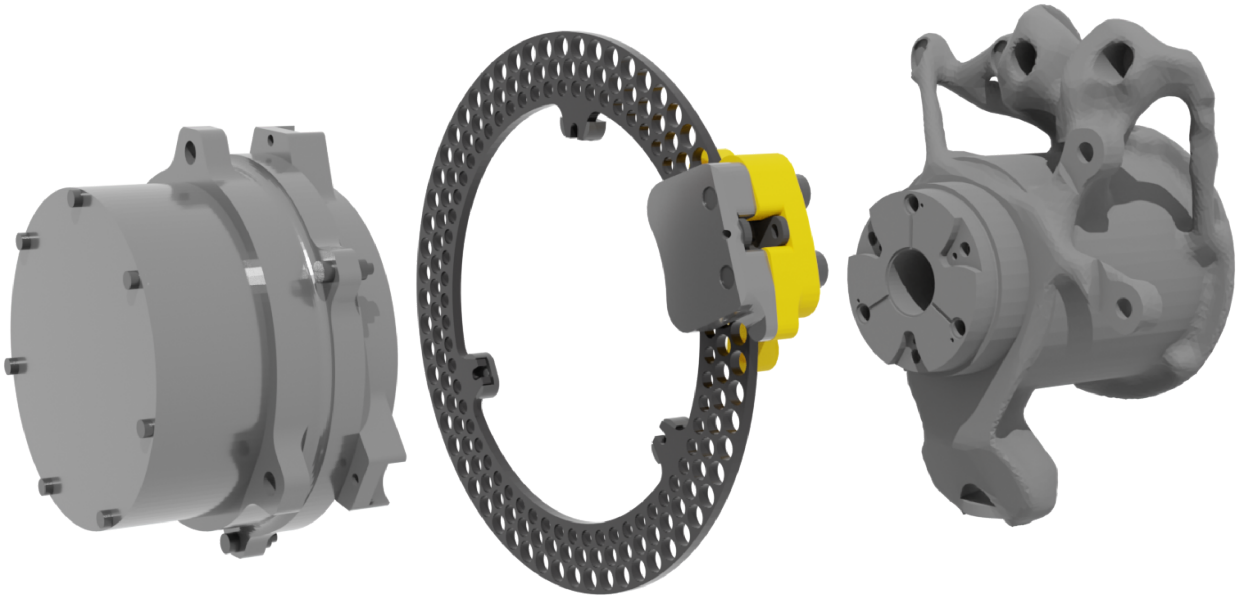

Development of a weight-optimized wheel assembly for a Formula Student car

Joel Hjalmarson
Erik Lydig
Gillian Makrof-Johansson
Gabriel Pfeiffer
Clemens Steinke
Anna Wrennfors

Department of Mechanics and Maritime Sciences

CHALMERS UNIVERSITY OF TECHNOLOGY
Gothenburg, Sweden 2023
www.chalmers.se

Supervisor: Björn Pålsson, Department of Mechanics and Maritime Sciences
Examiner: Håkan Johansson, Department of Mechanics and Maritime Sciences

Bachelor Thesis 2023
Department of Mechanics and Maritime Sciences
Chalmers University of Technology
SE-412 96 Gothenburg

Preface

We would like to express our sincerest appreciation to our examiner Håkan Johansson, and our supervisor Björn Pålsson for their support and external structure during the course of this bachelor thesis. We would also like to extend our gratitude to Herman Wäpling and Carl Thunberg for their technical support and guidance, as well as for providing the initial design concept on which the entire project was based. Lastly, we would like to thank the entire team of CFS23 for their collaboration, allowing us to work along them on key components of the vehicle.

Abstract

Formula Student is a global competition where university teams design, build, and race their own Formula-style race cars. The competition evaluates the design and performance of the cars through both static and dynamic events. The use of electric hub motors in the Chalmers Formula Students' car allows for greater handling but at the cost of an increase in unsprung mass. To extract the maximum performance, it is beneficial to minimize this mass, and in an attempt to do so, competing teams have started integrating parts of the wheel assembly. This paper investigates the possibility of combining parts in Chalmers Formula Students' wheel assembly as well as other methods to save weight. To achieve this, topology optimization, finite element analysis, and computational fluid dynamics softwares are used to evaluate and compare generated concepts. The results show that it is beneficial to combine parts of the wheel assembly, especially from a weight-saving perspective. The overall weight reduction per wheel assembly is 26%, which corresponds to a decrease of 5.3 kg for the entire car.

Keywords: Chalmers Formula Student, CFS, wheel assembly, upright, topology optimization, gearbox, cooling jacket, brake caliper.

Acronyms

CAD	Computer-Aided Design
CFD	Computational Fluid Dynamics
CFS22	Chalmers Formula Student 2022
CFS23	Chalmers Formula Student 2023
CFS24	Chalmers Formula Student 2024
CNC	Computerized Numerical Control
COP	Carry-Over Part
EV	Electric Vehicle
FDM	Fused Deposition Modeling
FEM	Finite Element Method
FSG	Formula Student Germany
SLS	Selective Laser Sintering

Contents

1 Introduction

Formula Student is one of the largest engineering competitions in the world with over 800 registered universities and teams [1]. The goal of the competition is for students to design, build, and race with an open-wheeled formula-style car. Each competition consists of multiple different static and dynamic events such as ”Endurance”, ”Skidpad”, and ”Acceleration”, where the teams test the limits of their vehicles to see who has designed the best race car [2].

Since 2003, each year Chalmers has partaken in various Formula Student competitions with its team Chalmers Formula Student. In the early days of the team, the cars utilized internal combustion engines and differentials for torque split. However, as technical development has progressed, cars nowadays use electric hub motors in each wheel assembly with individual control and torque vectoring [3]. This design allows for much greater control of the vehicle on track as well as greatly increased acceleration. But there is one clear drawback, the unsprung mass of the vehicle has increased. More unsprung mass makes it more difficult for the suspension system of the car to keep the tires in constant contact with the tarmac [4]. Therefore, Chalmers Formula Student now wants to reduce the mass of the wheel assemblies in order to find further performance.

The CFS wheel assembly consists of the following components: the upright, cooling jacket, gearbox, brake system, electric motor, and wheel, where the upright supports the whole structure, see Figures 1 and 2. The cooling jacket regulates the temperature of the motor whilst the gearbox transfers power from the motor, and the brake system decelerates the car.

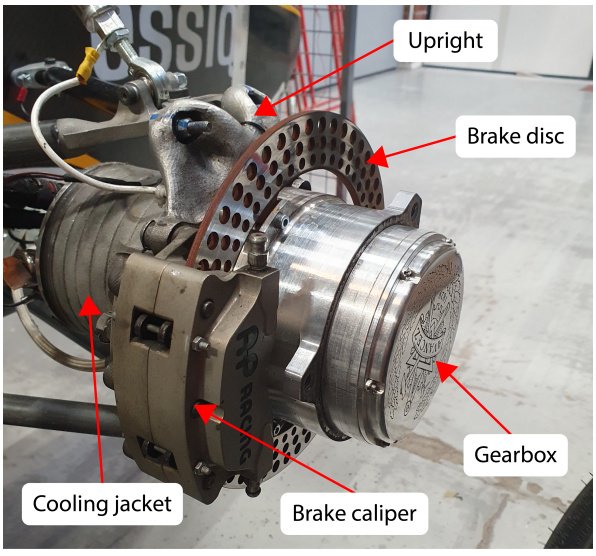

Figure 1: Wheel assembly outside.

Figure 2: Wheel assembly inside.

1.1 Cooling jacket

The motors in the CFS22 car must operate within a specific temperature range for maximum efficiency. During the conversion of electric energy to mechanical energy, inefficiencies cause some of the power to be converted to heat. This can lead to overheating which causes de-magnetization of the stator and decreases the performance [5]. The cooling system consists of water-filled channels that surround the motors, which transfer heat from the motors to the water. A pump moves the water through the cooling jacket's channels and past the power electronics, which also need cooling. Finally, the water flows to the radiators where the external air cools the water [6]. A section of the CFS22 cooling jacket is visualized in Figure 3.

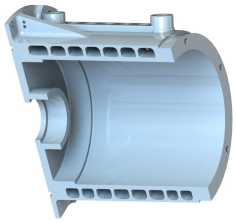

Figure 3: Section view of the cooling jacket from the CFS22 car.

The design of the cooling jackets impacts the entire cooling system, due to the pressure drop (ΔP) over the cooling channels. A reduction in pressure drop would mean a higher flow rate of the coolant, hence an increased cooling performance for the rest of the system. To achieve a low-pressure drop it is beneficial to have a slow-moving coolant, a short travel length with a small wetted perimeter in relation to the cross-sectional area [7]. The wetted perimeter is the perimeter of the cross-section normal to the flow direction.

The heat convection from the solid part to the coolant follows this governing equation:

$$\dot{Q} = A\alpha(T_{solid} - T_{fluid}) \tag{1}$$

Where α is the heat transfer coefficient and A is the boundary area between the fluid and cooling jacket (solid) [8]. Given a heat transfer $\dot{Q}$ in equation 1, assuming a constant α and constant fluid temperature T_{fluid} it is clear that to achieve a small T_{solid}, A needs to be large. A large A means a large wetted perimeter or long pipe, which as previously discussed gives a high-pressure drop. Therefore it is not possible to minimize the pressure drop and at the same time minimize the temperature of the cooling jacket, so a compromise must be made.

1.2 Gearbox

The electric motors in the CFS22 car are rated for 20,000 RPM and a speed reduction is therefore required to achieve the proper torque and top speed for the wheels. This is done with a compound planetary gearbox, which consists of three types of gear; a sun gear, planet gears in a compound arrangement, and a ring gear [9]. The combined gear reduction is 13:1, meaning that the motor must spin 13 revolutions for every revolution at the wheel.

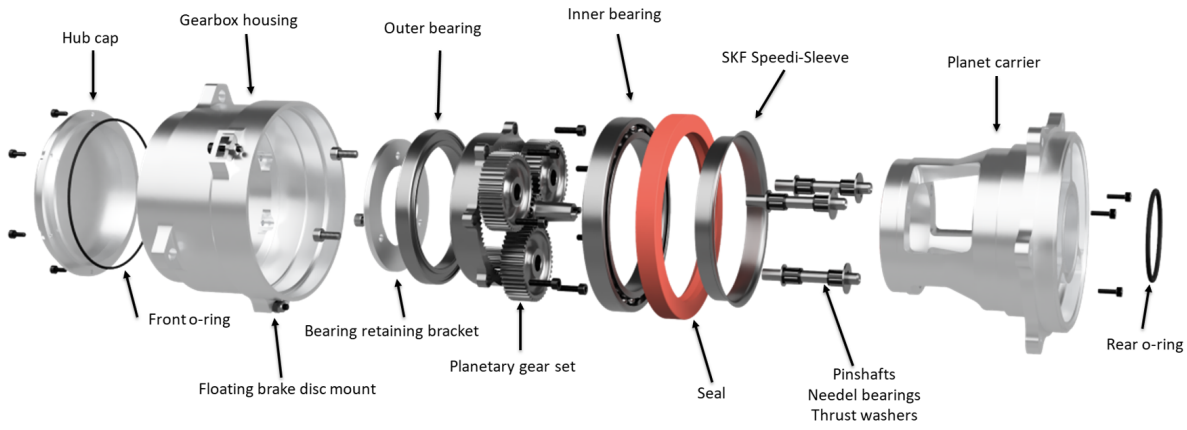

Figure 4: Gearbox assembly from the CFS22 car [10].

1.3 Brake system

The brake system on the CFS car uses a floating brake disc and double-acting brake calipers for both the front and rear wheels. A double-acting brake caliper has pistons on both sides of the brake disc, on the contrary, a single-acting caliper only has pistons on one side of the brake disc. A floating brake disc refers to the mounting solution, which allows certain axial travel while still being fixed around the axis of rotation. Though the axial travel is very small, it is enough to compensate for any warping of the brake disc or uneven wear on the brake pads.

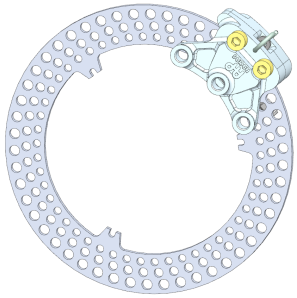

Figure 5: Rear brake disc and caliper from the CFS22 car.

1.4 Upright

The upright is the main structural component of the wheel assembly to which the upper and lower control arms are attached. The purpose of the control arms is to connect the wheel hub to the chassis. Other components such as the motor, gearbox, suspension members, and brake system are also mounted to it. The uprights have in the previous years gone from being CNC machined, to being manufactured using additive methods as their complexity has increased. The upright from CFS22 is visualized in Figure 6.

Figure 6: Upright from the CFS22 car.

2 Purpose

The purpose of this project has been to develop a lighter wheel assembly compared to the CFS22 design, this could for example be done by integrating parts. The final goal is to have a complete CAD model of the CFS24 wheel assembly along with all the necessary documentation and files needed for the next Chalmers Formula Student team to continue development. The concept must therefore be manufacturable and easily modifiable whilst staying within the limitations stated in 2.1.

2.1 Limitations

There are both internal and external limitations to the project. The internal limitations are given by the geometries and requirements of the components from previous years that will not be redesigned. These include motors, gears, wheels, and the positioning of the suspension linkages. Concerning the cooling of the motor, the whole cooling system will not be investigated, only the cooling jacket. The design will also be limited by the available materials and manufacturing methods. These materials will primarily be aluminium and steel alloys along with some non-metal materials like plastics and composites. The main manufacturing methods available are CNC milling and SLS metal 3D printing. Additional manufacturing methods such as FDM printing or laser cutting may be used.

Other internal limitations in the design, as stated by CFS22, are standardization of wheels, motors, cooling channels, and gearboxes across all four wheels to simplify the manufacturing process and the availability of components and spare parts. The motor and wheels are carry-overs from the CFS22 car and therefore will not be considered in the design process.

The external limitations are defined by the rule book from Formula Student Germany since this acts as the foundation for other European competitions [11]-[12]. Although the parts designed in this project are meant to be used in 2024, the project will follow the 2023 rule book since this is the most recently released version [2].

2.2 Research question per component

The sub-systems in the wheel assembly have their separate question formulations leading to the common goal of reducing the mass and complexity, whilst also improving manufacturability.

2.2.1 Cooling jacket

A target for the cooling jacket is to minimize its impact on the rest of the cooling system, which means that the pressure drop should be minimized. Another target is to reduce the weight of the cooling jacket, including the coolant. At the same time, the maximum temperature of the motor must not exceed the maximum allowed temperature. The cooling jacket will thereby be investigated with the following question:

- Can the weight of the cooling jacket, including the weight of the coolant, and the pressure drop be reduced, while still keeping the motor within its temperature limits?

2.2.2 Gearbox

In CFS22, the two bearings in the gearbox are over-dimensioned and the possibility of reducing the size of these will therefore be investigated. Currently, the planet carrier is outsourced and manufactured in a 5-axis CNC mill. If the design is simplified it could instead be manufactured in-house using a 3-axis CNC mill, thus reducing cost. The focus on the gearbox is to design after the following questions:

- Could the bearing size be reduced and still fit with the current gears?
- How could the planet carrier be redesigned for manufacturing in a 3-axis CNC mill?
- Would it be possible to integrate parts of the gearbox with the cooling jacket and upright to reduce weight?

2.2.3 Brake system

As the overall purpose of the project is to reduce weight, both brake calipers and brake discs will be investigated to see if it is possible to reduce their mass. More specifically the following points will be investigated:

- Could the mass of the brake disc be reduced while still maintaining sufficient braking performance?
- Would switching from the currently used double-acting brake calipers to single-acting brake calipers be beneficial without compromising performance?

2.2.4 Upright

The potential of additive manufacturing allows for more complex designs without adding a lot of extra complexity to manufacturing. In previous years, this potential has been utilized to minimize the mass of components such as the upright. Further performance gains using additive manufacturing will be investigated in the new design.

- What components of the wheel assembly could be integrated into the upright; and what would be the advantages and disadvantages of integrating more components in terms of complexity, stiffness, and mass?

3 Method

This project has used topology optimization for the upright and a product development methodology for the cooling jacket, gearbox, and brakes, which have influenced every step of the design process [13]. All the steps have been implemented separately for each of the sub-systems with regard to the compatibility of the other parts. A literature study was performed to provide benchmarking of existing technologies. After the literature study was performed a set of requirements was defined with the fundamental criteria to ensure all the functions of the wheel assembly are fulfilled. During a brainstorming session ideas were generated for each sub-system, which were compared and the most promising concept was further developed. After a final concept was chosen it was tested through simulations in different software.

3.1 Preliminary research

In order to gain a better understanding of the system it was divided into smaller subsystems; upright, cooling jacket, gearbox, and brakes. Relevant literature and solutions from other competing teams were studied for each sub-system and used as reference material for the brainstorming sessions.

In order to explore solutions developed by other teams, the group analyzed publicly available videos from competing teams, showcasing their latest designs and innovations. However, as all teams aim to maintain a competitive edge, not all design specifics were disclosed in these presentations. To further investigate, the group studied public photo albums, published by the competition organizers, that documented inspection events during the competitions. These photos revealed more design details that the teams otherwise would not have shown.

To ensure the quality of the concepts, a requirement specification was formulated. For a concept to be acceptable it had to meet all requirements in the specification. The specifications were defined based on multiple different sources, for example, load cases from CFS testing, manufacturability, and governing regulations.

3.2 Idea generation and filtering of concepts

During the brainstorming sessions, project members proposed new solutions for each sub-system and identified potential problems. These ideas were then cross-referenced using a morphological matrix to generate various concept combinations. Each concept was evaluated based on the requirements specification and compatibility with other sub-systems. Any concepts that did not meet the requirements or were incompatible were eliminated. This process helped identify the most feasible and effective solutions

for each sub-system.

3.3 Detailed design of concept

The detailed design of the concept was created using an iterative design process. To continuously evaluate the design, weekly design reviews were held with the supervisors and allowed the project group to iterate the concept many times during the design phase. Different types of resources were required to design a final concept that fulfilled the requirement specification and is listed in Table 1.

Table 1: Resources required for the project.

Resource	
Computer-Aided Design	Siemens NX for the design of wheel components and assemblies, Catia V5, and ANSYS SpaceClaim for complex surface modelling. Siemens Teamcenter for file sharing and version control.
Fluid analysis	STAR-CCM+ by Siemens was used for simulating CFD problems. The reason for this choice is that Chalmers Formula Student already uses the software for all other CFD.
Structural analysis	ANSYS for evaluating the mechanical properties of designed components, as it is already familiar to CFS and the project group.
Topology optimization	ANSYS Design Optimization Toolbench for easy iteration of designs, optimization, post-processing, and structural validation all in the same software.

3.4 Topology optimization

The topology optimization tool is used in combination with the possibility to manufacture the part with additive manufacturing. The design process began with defining a design volume using CAD. The design volume refers to the geometric shape which the topology optimization algorithm optimizes based on several load cases, see Chapter 4.3. The geometric shape is defined by the boundaries of where it can occupy space without clashing with the boundaries of the assembly parts. Thereafter FEM software was used to simulate the load cases affecting the wheel assembly. The solutions from FEM simulations were then transferred into the topology optimization tool which refined the

design volume to attain the desired retain percentage. The retain percentage is the proportion of the control volume that should be retained in the optimized part. The process of optimizing the control volume began with a coarse mesh to validate a rough shape of where the load routes were, to then be able to refine the design volume and minimize the number of mesh nodes. The topology-optimized part was then cleaned up by using post-processing tools and checked for clashing in the complete assembly. These steps were iterated with different parameters until the final concept was completed.

3.5 Validation of result

All sub-systems were validated using FEM to measure requirements such as stress, deformation, and buckling. The cooling jacket was also validated in STAR-CCM+ to measure flow and thermal behaviors.

4 Requirements

This chapter describes a set of requirements and specifications along with all calculations and reasoning that lead to the definition of all requirements.

4.1 Requirements and specification

In Table 2 all the requirements for the final concept are listed. R/W in the table stands for Requirement/Wish.

Table 2: Requirements and specifications.

Chalmers		**Requirement**	**Specification**		
Issuer: CFS			*Created:*	*230120*	
Requirement		Target Value	R/W	Verification	Ref.
1.	**Compliance**				
1.1	Camber (incl. rim)	$< 0.33°$	R	FEM Simulation	CFS
1.2	Toe	$< 0.14°$	R	FEM Simulation	CFS
2.	**Design loads**				
2.1	Withstand CFS23 loads see Chapter 4.3		R	FEM Simulation	CFS
3.	**Material**				
3.1	Safety factor (stress)	> 1.5	R	FEM Simulation	CFS
3.2	Heat resistant	$> 110°C$	R	Material choice	CFS
3.3	Max stress Aluminium 7075	< 286 MPa	R	FEM Simulation	CFS
3.4	Max stress AlSi10Mg	< 166 MPa	R	FEM Simulation	CFS
3.5	Max stress Hardox Hitemp steel	< 550 MPa	R	FEM Simulation	CFS
4.	**Size**				
4.1	Fit within the CFS23 rim diameter	< 240 mm	R	CAD estimation	CFS

4.2	Fit the CFS23 motors	d = 90 mm	R	CAD estimation	CFS
4.3	Fit within the CFS23 gears	1:13 reduction	R	CAD estimation	CFS
4.4	Fit with the CFS23 suspension geometry	CFS23 pickup points	R	CAD estimation	CFS
4.5	Distance from motor backside to rim interface	< 200 mm	R	CAD estimation	CFS
5.	**Rules compliance**				
5.1	T 6.1 Brakes		R	CAD estimation	CFS
5.2	T 7.2 Coolant fluid and system sealing		R	CAD estimation	CFS
5.3	T 7.3 Drive Train Shiels and Guards		R	CAD estimation	CFS
5.4	T 10.1 Critical Fasteners		R	CAD estimation	CFS
5.5	T.10.2 Securing Fasterners		R	CAD estimation	CFS
5.6	EV 3.1 Grounding		R	Materials choice and design	CFS
6.	**Manufacturability**				
6.1	Manufacturable with: 5-axis CNC, SLS metal 3D printing, waterjet cutting		R	Design choice	CFS
6.2	Manufacturable with: 3-axis CNC, SLS metal 3D printing, waterjet cutting		W	Design choice	CFS
7.	**Cooling jacket**				
7.1	Pressure drop per motor	< 2 kPa	R	CFD estimation	CFS

7.2	Pressure drop per motor	< 1.5 kPa	W	CFD estimation	CFS
7.3	Cooling performance per motor	0.9 kW	R	CFD estimation	CFS
7.4	Coolant liquid	Water	R	Material choice	CFS
7.5	Coolant liquid temperature	< 85°C	R	CFD estimation	CFS
7.6	Cooling jacket inner wall temperature	< 85°C	R	CFD estimation	CFS
8.	**Brakes**				
8.1	Brake torque per front wheel	> 350 Nm	R	Calculations	CFS
8.2	Brake torque per rear wheel	> 175 Nm	R	Calculations	CFS
8.3	Brake caliper passive side flex	< 0.35 mm	R	FEM Simulation	CFS
8.4	Max temperature of brake fluid	< 240°C	R	Calculations	CFS

4.2 Compliance

The toe angle refers to how much the wheels are rotated towards each other in the horizontal plane, and the camber angle refers to how tilted the wheels are in the vertical plane. The compliance requirements provided by CFS are based on the accuracy which is used to set the initial toe and camber angles. The compliance requirement includes all components between the tire and the chassis, such as the rim, gearbox, upright, and linkages. The rims contribute to a deformation equivalent to 0.15° camber change during hard cornering, but the effects on the toe compliance could be neglected [14]. The compliance of the linkages was calculated by hand, see Appendix 7.4.1, and the results for the final concept are presented in Table 14. Accounting for the compliances that the project can not affect, the gearbox and upright assembly has to stay below 0.17° deformation in the camber direction, and 0.14° in the toe direction.

4.3 Design loads

The load cases used to dimension all components are derived from the overall load cases of each wheel assembly, presented in Tables 3 and 4. The overall load cases were defined by CFS23 and the loads do not include any safety factor [15].

In the tables below, "Acc." refers to maximum acceleration, "Braking" refers to maximum braking, "Cornering" refers to the vehicle turning as hard as possible without losing grip, and "Bump" refers to the wheel rapidly being forced upwards due to passing over a bump in the road surface. The loads are given as the force in the contact patch of the tire. Positive x-direction is the forward direction of the vehicle, positive y-direction points to the left, and positive z-direction points upwards.

Table 3: Load cases for the front right wheel assembly.

Worst loadcase	F_x (N)	F_y (N)	F_z (N)
Acc. + Bump	1536	0	3178
Braking + Bump	-2418	0	3178
Cornering + Bump	0	3034	3178
Cornering + Acc. + Bump	1086	2145	3178
Cornering + Braking + Bump	-1710	2145	3178

Table 4: Load cases for the rear right wheel assembly.

Worst loadcase	F_x (N)	F_y (N)	F_z (N)
Acc. + Bump	1536	0	3524
Braking + Bump	-1323	0	3524
Cornering + Bump	0	3034	3524
Cornering + Acc. + Bump	1086	2145	3524
Cornering + Braking + Bump	-936	2145	3524

4.4 Fatigue life calculations

To get an estimate of how many load cycles Chalmers Formula Students' cars typically go through during their lifetime, an estimate of the distance driven in a complete season as well as the frequency of various load cases are needed.

4.4.1 Distance driven

A full season consists of three major parts, the pre-season testing, the competitions, and the post-season testing. There is very limited data on distance driven each season. However, Table 5 presents the total distance driven each season since 2016 as recalled by CFS alumni Christian Svensson and Mattias Naarttijärvi, as well as the team's faculty advisor Björn Pålsson.

Table 5: Kilometers driven each season.

Year	**Kilometers driven**
2022	350 km
2021	100 km
2020	0 km (*Due to Covid-19*)
2019	100 km
2018	300 km
2017	300 km
2016	700 km

An estimate of the total distance driven is therefore less than 350 km for each of the four last cars that CFS has built. However, CFS has proven in the early days of the EV era that upwards of 700 km is feasible. With a safety factor of slightly below 1.5, the conclusion is therefore that the fatigue-wise worst case is that the total distance travelled is roughly 1000 km per season. Given that the wheel assembly could be carried over for two or three seasons, the total distance travelled in a life cycle should be 3000 km.

4.4.2 Measured data from testing

Using available test data from CFS22, an estimate could be made of the various load cases that systems experience, and the frequency of each load case. The track the test data was gathered on was a 3 km long auto-cross track with a design based on the guidelines from the FSG rules book [2]. During the tests, a load cell was mounted in line with the front right pushrod, measuring the compression forces. The vehicle also logged many other parameters such as acceleration and velocity in all three directions, torque and speed of all four motors, and the position of the vehicle on the track. Using the force and acceleration data, the forces acting on the wheel assembly were calculated using Newton's second law, knowing the mass of the vehicle. The forces could then be broken down into components using trigonometry and the known angles of the suspension geometry.

The number of occurrences for each load amplitude is presented in Figure 7 below, separated into one histogram per direction. It is important to note that the Y-axis was scaled from the 3 km available test data to the 3000 km life cycle of the wheel assembly. As expected from the basics of vehicle dynamics, the distribution in the bar graph is not symmetric, for example, braking results in higher forces than acceleration.

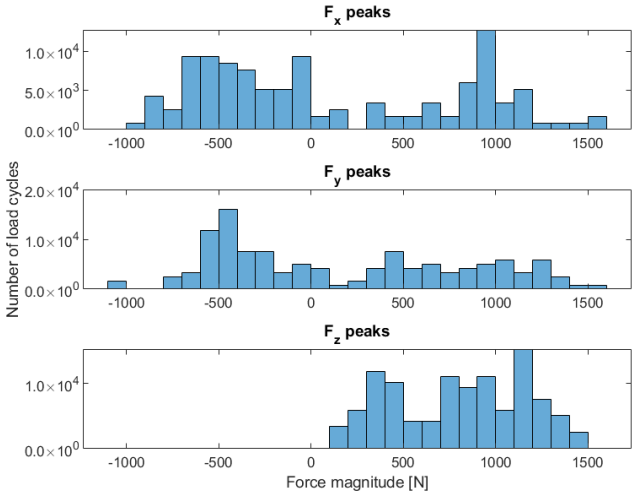

Figure 7: Number of occurrences of each load during a life cycle of 3000 km (front right wheel).

4.4.3 Fatigue for non-rotating components

Since the load cycles are not fully reversed but instead vary rapidly, all positive and negative peaks will be counted as complete reversed load cycles for a worst-case estimate. This shows that the combined number of load cycles, regardless of amplitude, remains below 10^5. The fatigue curve for $AlSi_{10}Mg$ acts too stochastic to be reliable for fatigue of less than 10^6 cycles [16]. Therefore, the additively manufactured component will be dimensioned according to the maximum allowed stress of 100 MPa to survive 10^6 load cycles instead.

4.4.4 Fatigue for rotating components

Rotating components in the gearbox go through approximately 2,3 million revolutions in the designed lifetime, where every rotation is one fully reversed load cycle. Given the number of load cycles and the fatigue curve for aluminium 7075 T6, the maximum allowed stress is 200 MPa [17].

4.5 Material properties

According to the manufacturer's datasheet for 3D-printed $AlSi_{10}Mg$ the yield strength is 250 MPa in the heat-treated state [18]. To achieve a safety factor of 1.5, stresses in 3D-printed components may not exceed 166 MPa. Similarly, for components CNC-milled in aluminium 7075 T6, the yield strength is in the span of 430-480 MPa and is therefore dimensioned to 286 MPa. Finally, any components made from Hardox Hitemp steel will have to be dimensioned to no more than 733 MPa in yield strength and a maximum temperature of 500°C.

5 Concept designs

This chapter presents the concept combination, evaluation, and the selected concept for each sub-system separately. For all sub-systems except the upright, the design process starts with a concept combination, followed by an evaluation of the generated concepts. The final concept of each sub-system is also presented in their respective sub-chapter, with an evaluation of the combined final product being presented at the end of the chapter. The upright does not have a concept combination or evaluation chapter since the use of topology optimization was set from the start of the project.

5.1 Cooling jacket

The different concepts for the cooling jacket will be presented and evaluated in this chapter. The final concept will also be shown and compared to the current CFS22 design.

5.1.1 Concept combination

In the idea-generation phase, the concepts were divided into three groups; channel concepts, inner wall concepts, and port concepts. The groups were used to break down the design into different regions of the cooling jacket that were independent of each other, see Figure 8. To generate the concepts, a morphological matrix was used which can be found in Appendix 7.2.1.

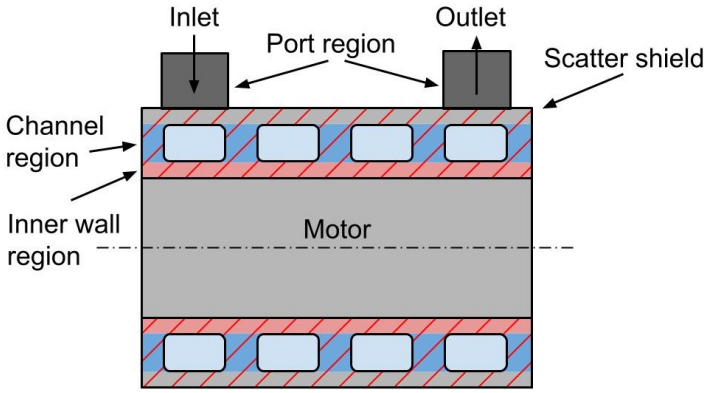

Figure 8: The different regions of the cooling jacket.

Some of the generated concepts for the channels utilized axially oriented channels. This means that the fluid flow is divided into a number of channels at the inlet side and merged back together on the outlet side. The advantage of this is that the parallel channels act as one big channel, which according to the theory presented in Chapter 1.1 results in a lower pressure drop, ΔP. These concepts are illustrated in Figure 9.

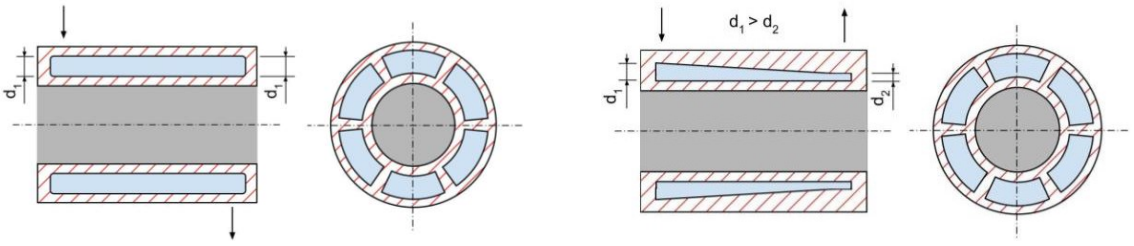

Constant channel cross section. Decreasing channel cross section.

Figure 9: Axial Channel concepts 5 (left) and 6 (right).

In contrast to the axial channels, the other main group of channel concepts has helical-shaped channels around the motor, see Figure 10. This design has many parameters that can be constant or vary along the length of the motor. Channel concept 1 is the simplest case of this concept, where both the width and the spacing of the channels are kept constant along the entire length. In an attempt to even out the temperature along the motor, Channel concept 2 has a varying channel width and Channel concept 3 has a varying channel spacing. Both these concepts aim to enhance the cooling effectiveness near the outlet of the cooling jacket, where the coolant will have reached a higher temperature. Finally, using the same idea, Channel concept 4 attempts to even out the temperature distribution by varying both the channel width and the spacing. Having a more even temperature distribution over the motor would increase its performance and ability to handle peak loads [19]. The reason for this is that the resistance of the copper windings, hence the magnetic field in the stator, varies with temperature [20]-[21]. The concepts can be viewed in Appendix 7.3.1.

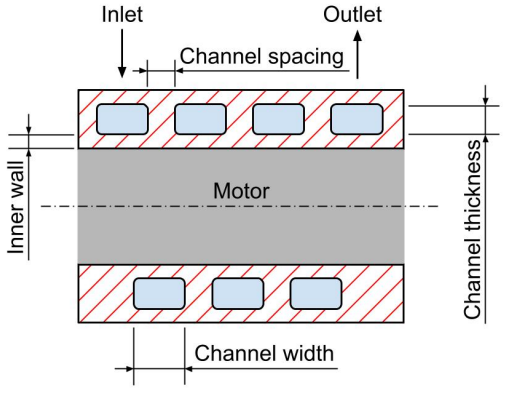

Figure 10: Section view of the general case of Channel concept 1-4.

For the port and inner-wall concepts, there were only two alternatives found for each. The ports could either be oriented perpendicular or tangential to the channels. Meanwhile, for the inner wall, the alternatives were to either have a 2 mm thick inner-wall

acting as a scatter shield or use the casing of the motor as the inner surface of the channels. The inner wall could not be thinner than 2 mm due to limitations in the manufacturing method, and thicker walls showed no benefit over the minimum required material thickness. The geometric differences between the concepts for the inner wall are illustrated in Figure 11.

Inner wall concept 1: Inner wall between channels and motor.

Inner wall concept 2: No inner wall between channels and motor.

Figure 11: Generated concepts for the inner wall.

5.1.2 Concept evaluation

The concepts were evaluated using the software STAR-CCM+ where water flow was simulated through the cooling jacket. The setup was designed to simulate the heat from the motor being absorbed and transported away by the coolant. In a real-world scenario, heat is also transported away from the cooling jacket through convection with the air, but according to Appendix 7.6.3 this effect was negligible. Therefore, the convection with the external air was not considered in the simulations. In order to ensure performance in all conditions, the heat loss of the motor when running at maximum capacity was used in the simulations. The coolant mass flow was considered to be constant, not taking changes in pressure drop into account. Also, the temperature of the coolant was set to be the same as at the end of an endurance run, to capture the maximum temperature. The simulation parameters used is given in Table 6

Table 6: Simulation data for the cooling jacket.

Property	**Numerical value**
Energy loss per motor	$900W$, Requirement 7.3
Density (Solid parts)	$2.67g/cm^3$ [18]
Specific heat capacity (Solid parts)	$900J/(KgK)$ [22]
Thermal conductivity (Solid parts)	$155W/(m*k)$ [18]
Coolant inlet temperature	$59.5°C$, Appendix 7.4.2
Coolant mass flow	$0.033kg/s$ [23]

When evaluating the channel concepts with axial channels it was noticed that the water flow through the axial channels was uneven, see Figure 12, where the majority of the water was flowing through the channels near the plane given by the in and outlet. As a consequence of this, the temperature distribution was uneven which resulted in a maximum inner wall temperature that was significantly higher than for the helical concepts (1-4). Achieving a uniform flow when splitting a channel is a complex problem with solutions that are very sensitive to imperfections and lead to a decrease in performance [24]. Therefore, both concepts with axial channels, Channel concepts 5 and 6, were eliminated.

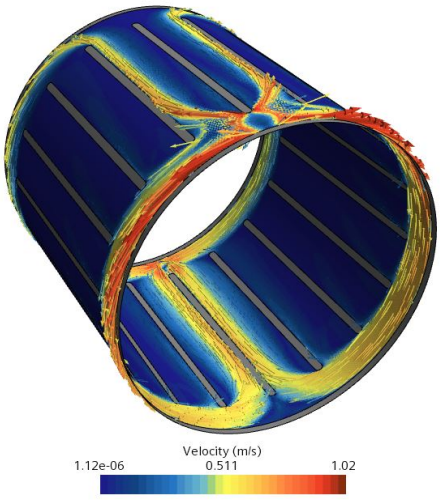

Velocity distribution.

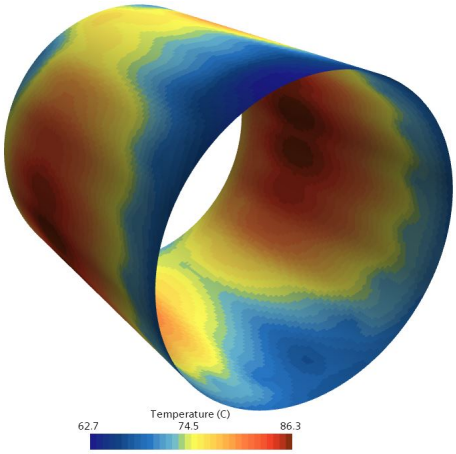

Temperature distribution on the inner wall.

Figure 12: Velocity and temperature distribution of Channel concept 5.

Looking at the helical concepts, it can be noticed that Channel concept 4 is a combination of Channel concepts 2 and 3. While this gives great controllability of the temperature distribution it also has many parameters that define the design, which

makes it complicated to optimize. Because Channel concepts 2 and 3 were considered to have enough ability to even out the temperature, whilst having significantly fewer parameters to decide, Channel concept 4 was eliminated.

The three concepts remaining are all using the helical channel design. The simulation results of these concepts are shown in Table 7, where T_{max} refers to the maximum simulated temperature on the inner surface towards the motor and ΔT refers to the temperature difference between the hottest and the coldest points on the mentioned surface. Table 7 also shows that Channel concept 1, using both constant spacing and channel width, performed worse in regards to both the maximum temperature and the difference in temperature over the cooling jacket. For this reason, Channel concept 1 was eliminated.

Table 7: Simulation data for Channel concepts 1-3.

Concept	$\boldsymbol{T_{max}(°C)}$	$\boldsymbol{\Delta T(°C)}$	$\boldsymbol{\Delta P(kPa)}$	**Mass incl. water (g)**
Channel concept 1	74.90	11.77	1.48	311
Channel concept 2	73.25	9.52	1.47	314
Channel concept 3	73.66	10.63	1.55	309

Figure 13 shows that both Channel concepts 2 and 3 have relatively similar temperature distributions. The only noticeable difference is that the coolant heats up faster in Channel concept 3, which smooths out the transition between temperatures. On the other hand, Table 7 shows that Channel concept 2 has a slightly lower maximum inner wall temperature and inner wall temperature delta.

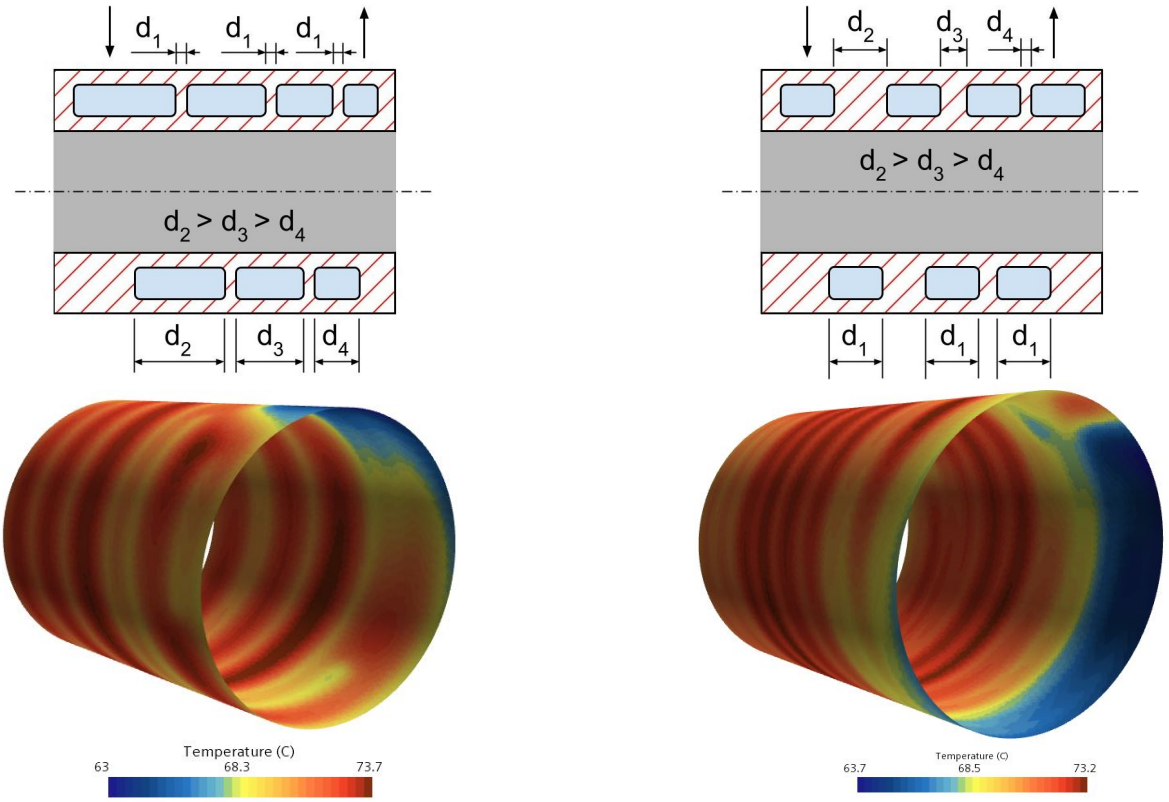

Channel concept 2. Channel concept 3.

Figure 13: Channel concepts 2 and 3 and their respective temperature distributions on the inner surface towards the motor.

Since Channel concepts 2 and 3 showed very similar performance, the focus was shifted to the flexibility and freedom of design that the two concepts could offer. Channel concept 2, with variable channel widths, proved to be easier to modify when fewer turns were used, because of its ability to reach the axial boundaries of the cooling jacket. Channel concept 3 on the other hand had trouble with overheating on these boundaries. The reason for this was that the channel got too far away from the axial boundaries when the pitch of the helix was increasing due to the fewer turns. Another benefit of Channel concept 2 compared to Channel concept 3 is the constant wall thickness since this reduces the risk of warping during additive manufacturing [25]. For these reasons, Channel concept 3 was eliminated and Channel concept 2 was chosen as the final concept.

The port concepts, visualized in Figure 14, were evaluated through simulations using the same channel layout and the same port diameter. The pressure drop for Port concept 1 was 8.58 kPa and 6.03 kPa for Port concept 2. Since Port concept 2 has a 30% lower pressure drop, this was chosen as the final port concept.

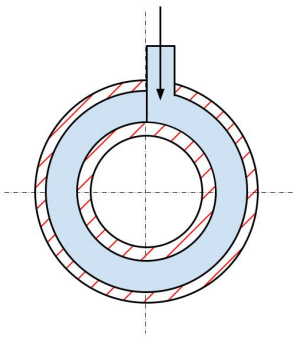

Port Concept 1.

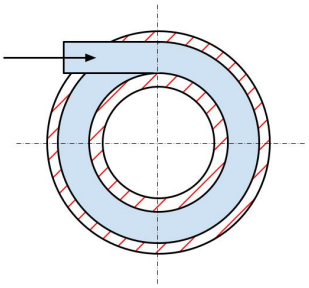

Port Concept 2.

Figure 14: Views of the port concepts.

The decision to eliminate the inner wall in the cooling jacket was based on two factors: weight reduction and design flexibility. Without an inner wall, each jacket would weigh approximately 140 g less, and the removal of excess aluminium powder from the 3D printing process would be simpler. However, this change also introduced a new complexity - the need for proper sealing to prevent leaks. Ultimately, the benefits of reducing weight and improving design flexibility outweighed the added complexity of adding sealing. As a result, the decision was made to proceed without an inner wall. The effect on the cooling performance of having an inner wall was simulated and shown to be negligible, see Appendix 7.6.2.

5.1.3 Final concept

The final cooling jacket concept has no inner wall, uses a helical channel, and the ports are tangential to the channel. The helical channel has a varying width and constant spacing. Even though the concept has been chosen, the following choices were still to be made: The number of helical revolutions, the thickness of the channels, and the varying pitch of the helix. Systematically evaluating these parameters showed that it is most beneficial to have a design with 3 helical rotations, a channel thickness of 3 mm, and a helix with a linear pitch of gradient 4. Figure 15 visualizes the final design using these parameters. For a discussion of why these parameters were chosen, see Appendix 7.6.1.

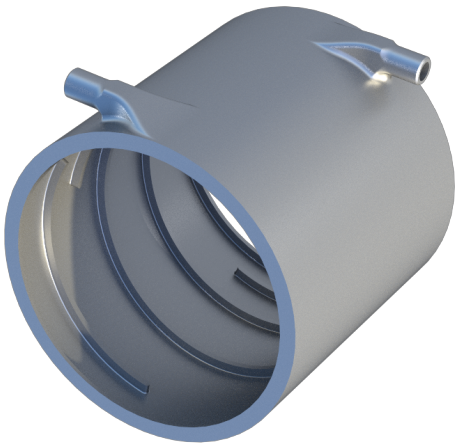

External view of the final design.

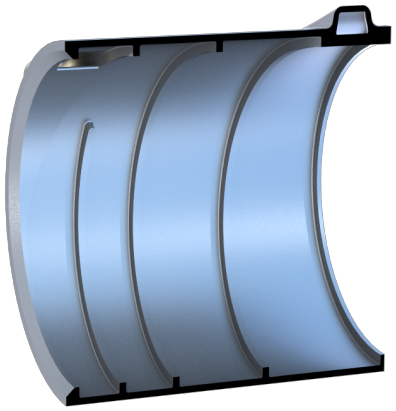

Internal view of the final design.

Figure 15: The final design of the cooling jacket.

Table 8 shows a comparison between the final concept and the CFS22 design without its structural parts, both being simulated with the parameters from Table 6. The new concept outperforms the old design in all listed categories except the maximum temperature on the inner wall. Although this temperature is higher, it is still well within the bounds of the specified requirements in Chapter 2.

Table 8: Data for the final concept compared to the CFS22 design without its structural parts.

Category	**CFS22**	**Final concept**	**Comparison (%)**
$T_{max,innerwall}(°C)$	72.96	74.55	+2.2%
$\Delta T_{innerwall}(°C)$	9.79	9.38	−4.2%
Pressure drop (kPa)	2	1.25	−37.5%
Mass incl. water (g)	629	280	−55%

The final concept has a more even temperature distribution on the inner wall compared to the CFS22 design, visualized in Figure 16, which as previously discussed is beneficial for the performance of the motor.

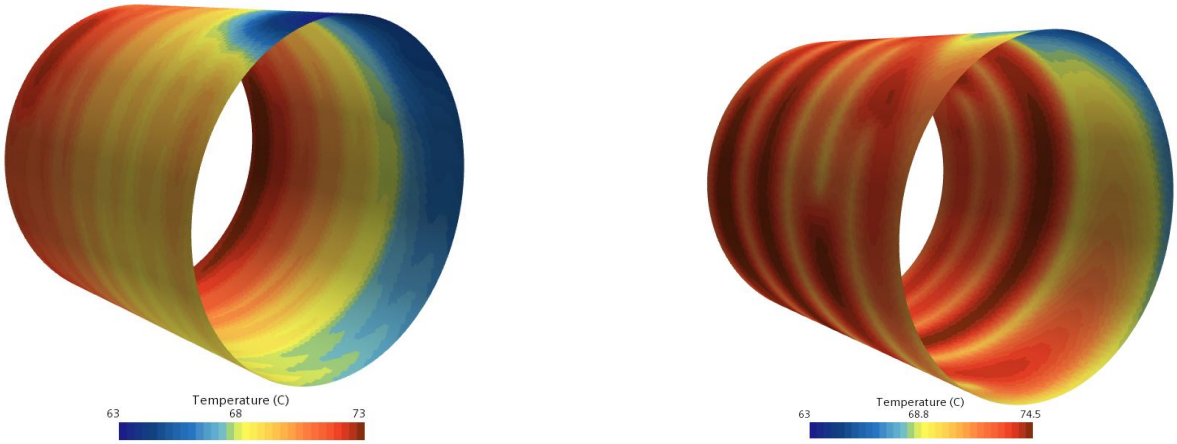

CFS22 design. Final concept.

Figure 16: Temperature on the inner wall of the CFS22 design and the final concept.

Since the concept does not have an inner wall, o-rings are used to prevent leakages, see Figure 17. The mounting of the motor is used to apply pressure on the o-rings and will be integrated as a part of the upright.

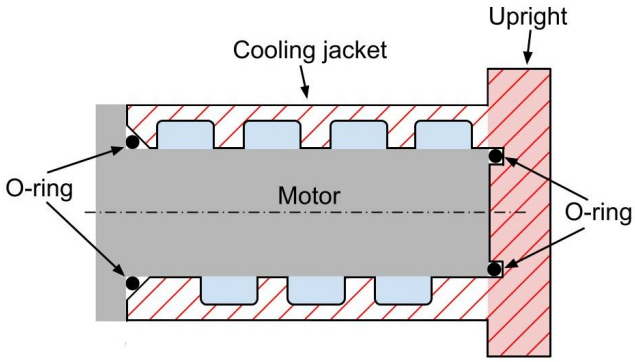

Figure 17: Placement of the two o-rings that prevent leakage from the cooling jacket.

5.2 Gearbox

All the generated concepts for the gearbox will be presented, evaluated, and a final concept will then be chosen. Lastly, the final concept will be compared to the CFS22 design.

5.2.1 Concept combination

A technical starting point received from the CFS alumni was to mount the planet carrier with bolts coming from the cooling jacket and upright as seen in Figure 18. This concept

will not be evaluated since the bolts will be hard to access when the motor is installed. Weight can instead be saved by integrating the planet carrier with the cooling jacket and upright.

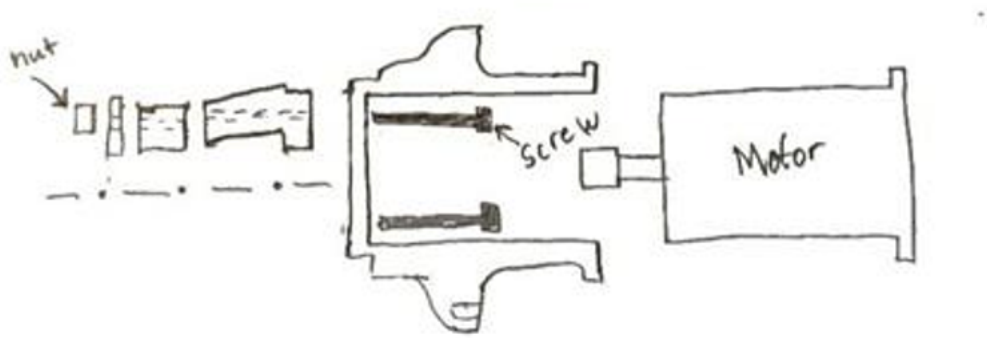

Figure 18: Technical starting point from CFS alumni [26].

In order to reduce the mass of the gearbox, the design was broken down into three sub-solutions; splitting the housing, splitting the planet carrier (PC), and flipping the gears axially. See Figure 19 for an illustration of the different sub-solutions. These solutions were then combined using a morphological matrix and eight concepts were generated. The morphological matrix and all the resulting concepts can be found under Appendix 7.2.2 and 7.3.2.

In Figure 19 the blue area represents the compound planetary gearset, the red area is the oil seal, the grey area is the bearings, and the black dashed lines indicate bolt holes. The motor and upright are integrated at the inner side of the gearbox.

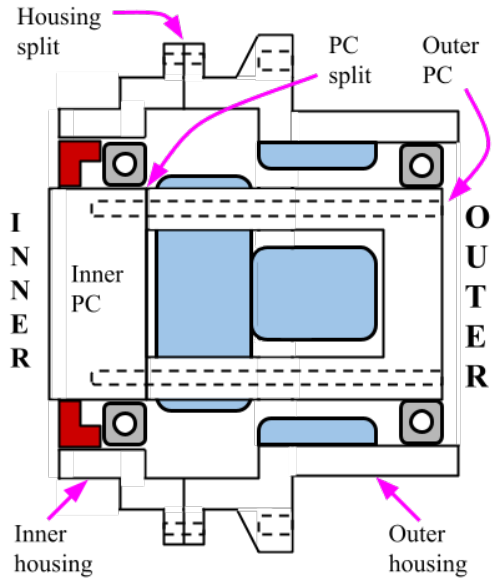

Concept 3: Two-piece housing, two-piece planet carrier, no flip gears.

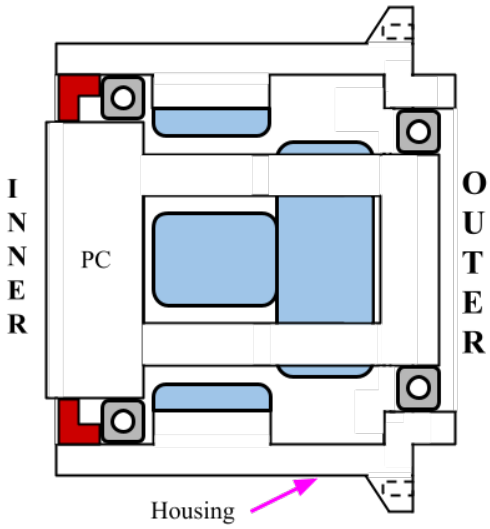

Concept 6: No two-piece housing, no two-piece planet carrier, flip gears.

Figure 19: Two concepts illustrating the combined solutions.

5.2.2 Concept evaluation

Simplified CAD models were used to test the fundamentals of the different concepts. As Figure 20 shows, flipping the gears would limit how far the rim can be pushed over the gearbox housing, resulting in a greater offset which is not desirable. Reducing the offset was stated as Requirement 4.5, therefore all concepts using flipped gears were eliminated, meaning Concepts 5, 6, 7, and 8.

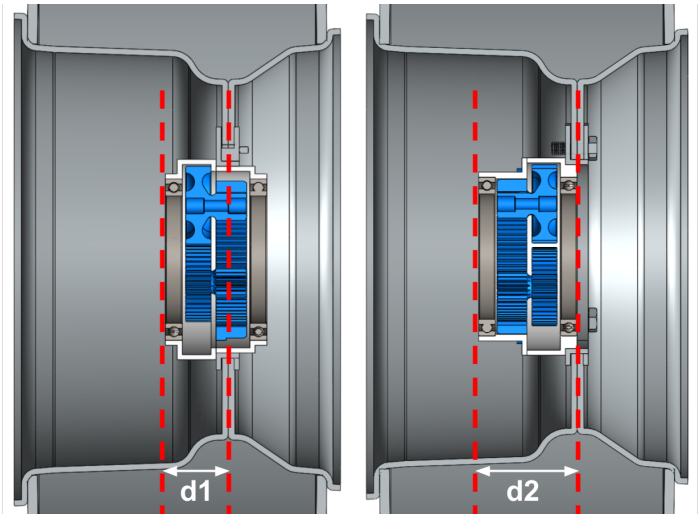

Figure 20: Section view displaying the offset difference ($d1 < d2$) between no flip gears (left) and flip gears (right).

The next step was to evaluate if splitting the planet carrier would be beneficial. The biggest downside of keeping the planet carrier intact is that its manufacturing would need to be outsourced to a company with 5-axis CNC milling capabilities. Splitting the otherwise complex component would allow for in-house manufacturing on 3-axis machines and therefore reduce manufacturing costs. A two-piece planet carrier would additionally offer improved accessibility and simplified assembly. For this reason, Concepts 1 and 2 were eliminated since they did not feature a two-piece planet carrier.

The remaining concepts are numbers 3 and 4, both of which utilize a split planet carrier. The benefit of also splitting the gearbox housing was evaluated based on detailed CAD analyses. The CAD models provided good estimates of each concept's possible mass, which supported the final decision. There were two criteria, mass, and manufacturability, that would determine which of the two concepts was to be developed further. The concepts were evaluated based on their trade-off between reduced mass and increased complexity. For an objective comparison, both needed to be finalized to a point where they had approximately the same deformation. This was done through iterative improvement of both designs until both reached acceptable deformations.

Figure 21 shows the comparable CAD models of each concept. By applying the corresponding material to the parts, their weights could be estimated, see Table 9. Concept 3's comparative weight savings of almost 300 g compared to Concept 4 outweighed its added complexity. Therefore Concept 3 was ultimately chosen for the final design.

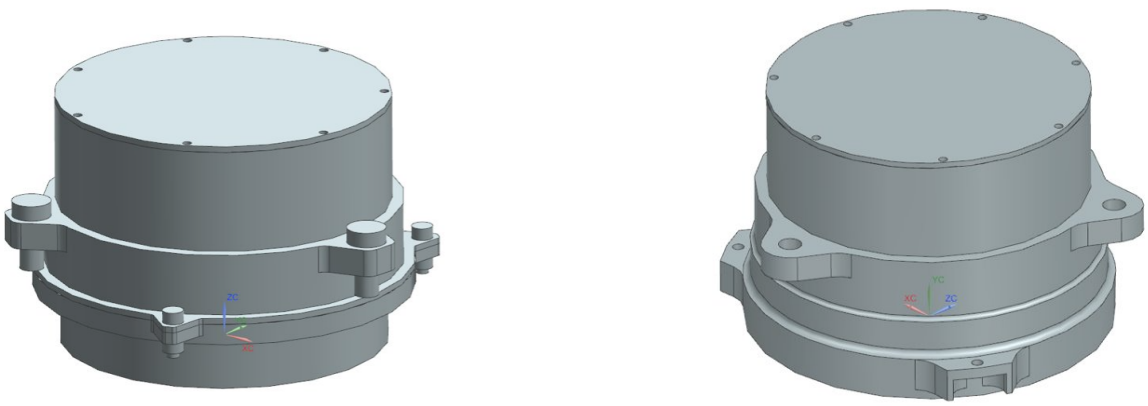

Figure 21: Early version of Concepts 3 (left) and 4 (right).

Table 9: Weight comparison between early concepts.

Component	**Concept 3**	**Concept 4**
Bottom planet carrier	249 g	425 g
Top planet carrier	194 g	194 g
Bearings	280 g	420 g
Housing	550 g	491 g
Fasteners	49 g	38 g
Speedi-sleeve	68 g	101 g
Total:	1 390 g	1 678 g

5.2.3 Final concept

The final gearbox concept consists of a split planet carrier, a split housing, and the gears in their original orientation, as presented in Figure 22 and 23. The inner part of the planet carrier will be integrated with the upright and cooling jacket, and therefore this component will be additively manufactured in AlSi10Mg. The remaining components, both housing halves, the outer planet carrier, and the hubcap will be machined using 3-axis CNC machines in aluminium 7075 T6.

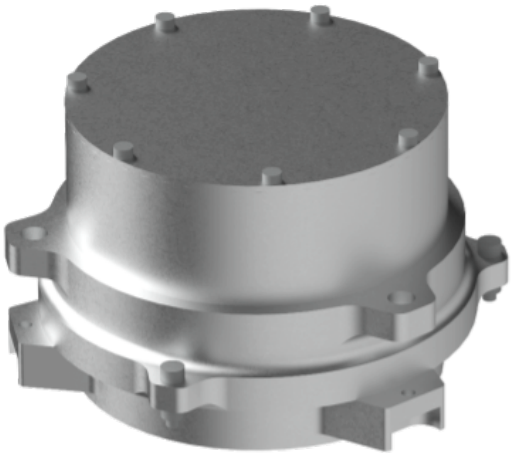

Figure 22: Isometric view of the final gearbox design.

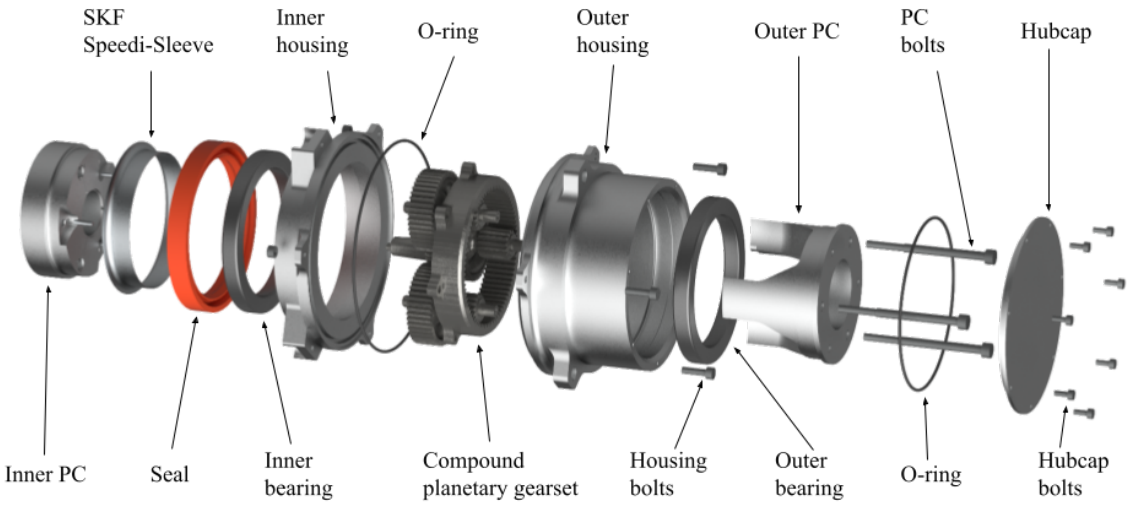

Figure 23: Exploded view of the assembled gearbox.

Because of the split housing, the size of the inner bearing, seal and speedi-sleeve could be reduced, resulting in further weight savings. Bearing calculations confirm that the bearings maintain their integrity throughout their entire lifespan, can be found in 7.4.5. Compared to the CFS22 gearbox, the final concept weighs approximately 412 g less per wheel, which means a total weight save of 1.65 kg in unsprung mass, see Table 10.

Table 10: Weight of final concept compared to CFS22 gearbox.

Component	**CFS22**	**Final Concept**	**Comparison (%)**
Planet carrier	649 g	473 g	-27%
Bearings	420 g	280 g	-33%
Housing	610 g	592 g	-3%
Hub cap	115 g	60 g	-48%
Gears	739 g	739 g	0% (COP)
Fasteners	39 g	49 g	+25%
Speedi-sleeve	101 g	68 g	-33%
Total:	2 673 g	2 261 g	-15%

FEM simulations were used continuously during the design to assure that each iteration improved relative to its predecessors. Not every load case listed in the requirements specification was tested for each iteration, in order to save computational time. However, all listed load cases were simulated for the final design as validation, see Appendix 7.7.

Due to the inaccuracies in simulating the local stresses and deformations around threaded fasteners, the simulations made simplifications in these areas and the strength of the threads was determined through hand calculations and physical testing, presented in Appendix 7.4.3, 7.4.4, and 7.5. Since the physical test was conducted with 5 mm thick walls around the thread, all simulated stresses in this region around threads will be disregarded.

During the worst load case simulation, it was found that the maximum stresses were located where the M5 bolts thread into the inner planet carrier. However, as mentioned above, these stresses could be disregarded and the stresses were therefore measured 5 mm away from the holes. Since the loads for the front and rear wheel assemblies differ, two sets of simulations were evaluated. Both simulations were evaluated below the maximum allowed stress with a magnitude of 51 MPa respective 59 MPa. The largest deformation was 0.082 mm and occurred during the worst load case in the front wheels, see Figure 24a.

The deformation in the gearbox plays a significant role in fulfilling the requirements of toe and camber compliance, which are specified in requirements 1.1 and 1.2. Figure 24b shows the directional deformation affecting camber and toe compliance, later presented in Chapter 6.

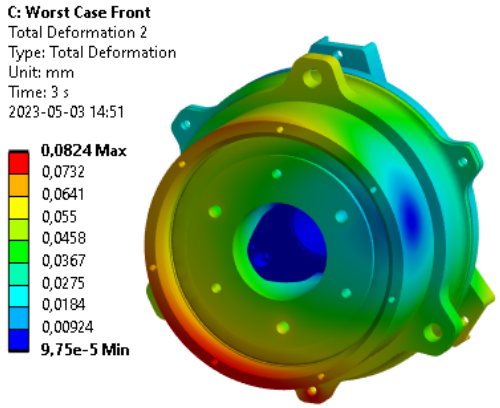

(a) Total deformation in gearbox during worst case.

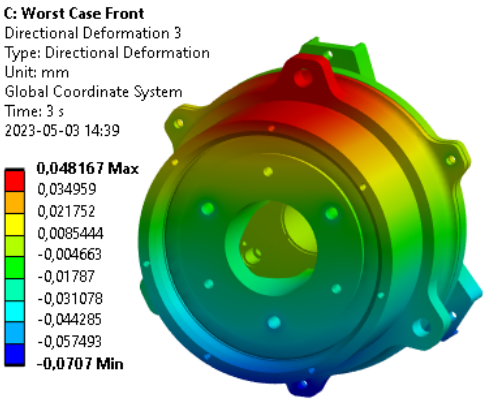

(b) Camber and toe deformation during worst case.

Figure 24: Deformation in the gearbox during the worst front wheel load case.

The gearbox housing is the only structural rotating part manufactured in aluminium 7075 T6 and should not exceed 200 MPa to avoid fatigue, as stated in Chapter 4.4.4. Simulations of braking and acceleration were carried out on the housing. Maximum stress during braking was 148 MPa, see Figure 25a, and 139 MPa during acceleration, see Figure 25b, confirming the housing will not fail due to fatigue.

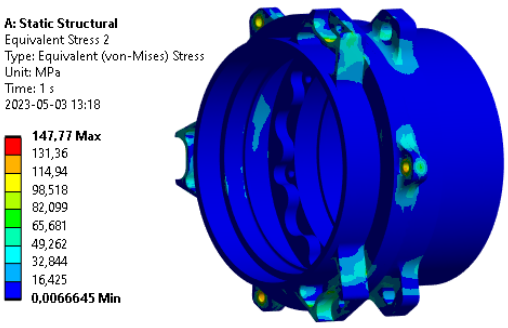

(a) Stress in gearbox housing during braking.

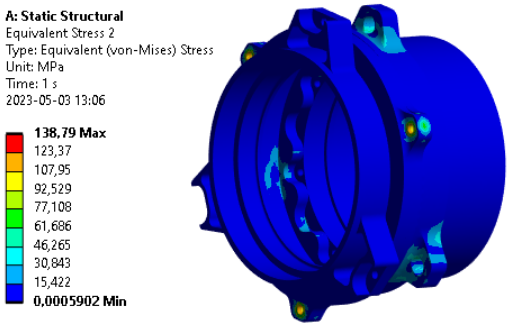

(b) Stress in gearbox housing during acceleration.

Figure 25: Stress in gearbox housing during braking and acceleration.

5.3 Brake system

Different concepts for the brake system will be presented and evaluated in this subchapter. Then, the final resulting concept is presented and compared to the CFS22 concept.

5.3.1 Concept combination

Similar to how the cooling jacket was broken down into separate sub-systems in the idea generation phase, the brake system was also broken down into three sub-systems. These were the caliper, the brake disc, and the position of the brake disc. The sub-systems were deemed independent of each other, and therefore no morphological matrix was used to combine them. All ideas generated are presented in Appendix 7.1.

Brake caliper concepts 1 and 4 make use of parts from the existing calipers, Concepts 2 and 3 include buying new calipers, and Concept 5 aims to integrate the caliper into the upright. As for the brake discs, there were only two concepts, either design and manufacture a disc in-house, or purchase a commercially available disc. Finally, for the three position concepts; Position concept 1 is mounting the brake disc on the motor side of the wheel assembly, see Figure 26a. Position concept 2, has the brake disc mounted directly onto the motor shaft, between the motor and gearbox, see Figure 26b. Finally, Position concept 3 is the one most commonly found in Formula Student cars. It has the brake disc mounted on the outside of the gearbox housing, see Figure 26c.

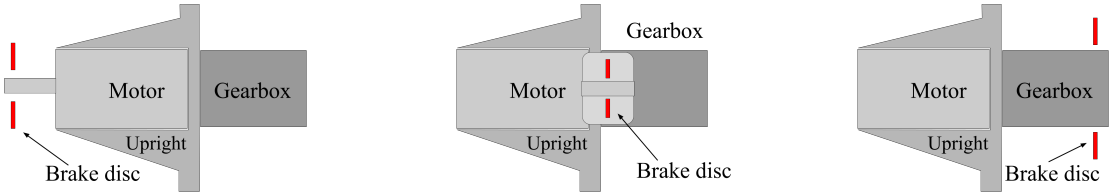

(a) Position concept 1. **(b)** Position concept 2. **(c)** Position concept 3.

Figure 26: Different brake disc position concepts.

5.3.2 Concept evaluation

When comparing single-acting calipers with double-acting calipers there are a few differences. Single-acting calipers have pistons on only one side of the brake disc while double-acting calipers have pistons on both sides. Both types offer similar braking performance, however, single-acting calipers can be made smaller and lighter since they only have pistons on one side. The drawback of single-acting calipers is that they require the brake disc to move axially as the brakes are being applied, this can on a Formula Student car be solved by using floating brake discs. Since both types of calipers offer similar performance and both are applicable to Formula Student cars, the double-acting concepts were eliminated due to their added weight.

Integrating the caliper into the upright would lead to a much more complex manufacturing process since the internal geometries of a caliper require high tolerances.

Another drawback was that if anything were to break on the caliper, the whole upright would have to be replaced. Therefore, Concept 5 was deemed infeasible and eliminated.

For the final comparison between buying a single-sided caliper or re-designing the current one, a market research was conducted. The research mainly included bicycle and motorcycle brakes, however, it was found that none of the single-acting brake calipers available on the market met all of the requirements. Thus, Concept 3 was eliminated in favor of the slightly more complex, but more flexible alternative of re-designing the current calipers.

The main difference between the brake disc concepts is their design freedom. A purchased disc limits both the packaging and optimization, forcing the gearbox housing to adapt instead of the disc. By designing custom discs, all parameters such as mounting positions, number of mounting points, outer and inner diameters, ventilation pattern, and thickness of the brake disc can be optimized. Since both waterjet cutting and CNC grinding are among the available manufacturing methods, new brake discs can easily be manufactured regardless of their final shape. Therefore the added manufacturing time was outweighed by the limitations of buying commercially available discs.

When it comes to the positioning of the brake disc, two out of three concepts can quickly be eliminated based on their added complexity in both design and manufacturing. Position concept 1 puts the disc in between the moving linkages which constrain the diameter to be significantly smaller, meaning larger forces are required for the same braking performance. Installing the brake disc inside the upright, between the motor and gearbox, requires an integrated brake caliper in order to reach the brake disc. Since the integrated brake caliper concept had already been eliminated, Position concept 2 was also eliminated. Therefore Position concept 3 will be used in the final concept.

5.3.3 Final concept

The final concept is to carry-over the current AP-racing calipers but convert them from double-acting to single-acting. The passive side, without a piston, will be an in-house manufactured component that supports the brake pads on the reaction side. Figure 27 illustrates the complete assembly of the front and rear calipers, including the new passive supports. The yellow and purple components are carry-over from the original AP-racing components.

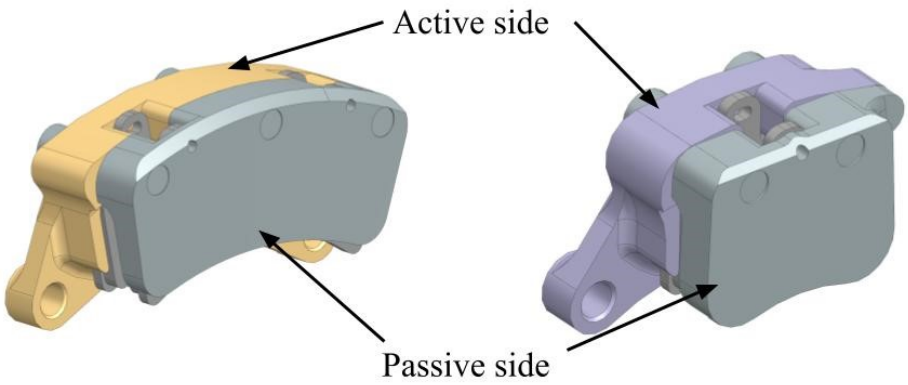

Figure 27: Final concept of the front brake caliper (left) and the rear brake caliper (right).

Due to the high forces that the passive sides of the calipers have to withstand, the strong, yet lightweight, aluminum alloy 7075 T6 was chosen. The benefits of this design and material are that it can be machined using 3-axis CNC mills, and the metal is already commonly used in CFS.

The final concept was simulated in ANSYS to find the largest deformations and stresses that occur under load. The simulations used the maximum force that can be expected during driving. Figure 28 illustrates the simulated deformation throughout both calipers' passive sides, showing that both meet the requirements for deformation.

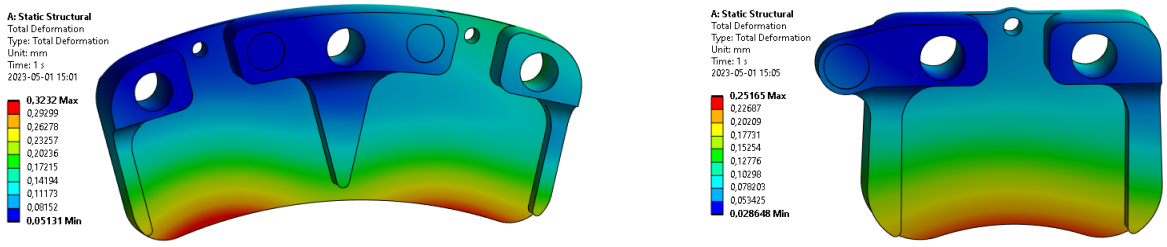

Figure 28: Resulting deformation for the passive sides of the front caliper (left) and rear caliper (right).

For the brake disc design, a collection of different designs were considered. Some designs are directional which is better at absorbing force in one direction over the other and others are rotationally symmetrical. The final brake disc was simulated for deformation and stress under load. The brake disc was also simulated for buckling, as this is an additional failure risk for the brake disc. The buckling simulations showed that neither the front nor the rear is at risk of buckling under braking. When determining

the thickness of each brake disc the heat generated from a heavy braking event was considered in addition to the other structural simulations. After considering all previously mentioned factors, the front and rear brake discs' final thickness resulted in 4 mm and 2 mm, respectively. In Figure 29 the maximum stress of both brake discs is visualized, the maximum stress in the front brake disc is 463 MPa, and 430 MPa in the rear brake disc. The remaining simulations are shown in Appendix 7.8. The brake discs will be made from Hardox Hitemp steel as it is a hard and strong alloy that will retain its hardness even at high temperatures.

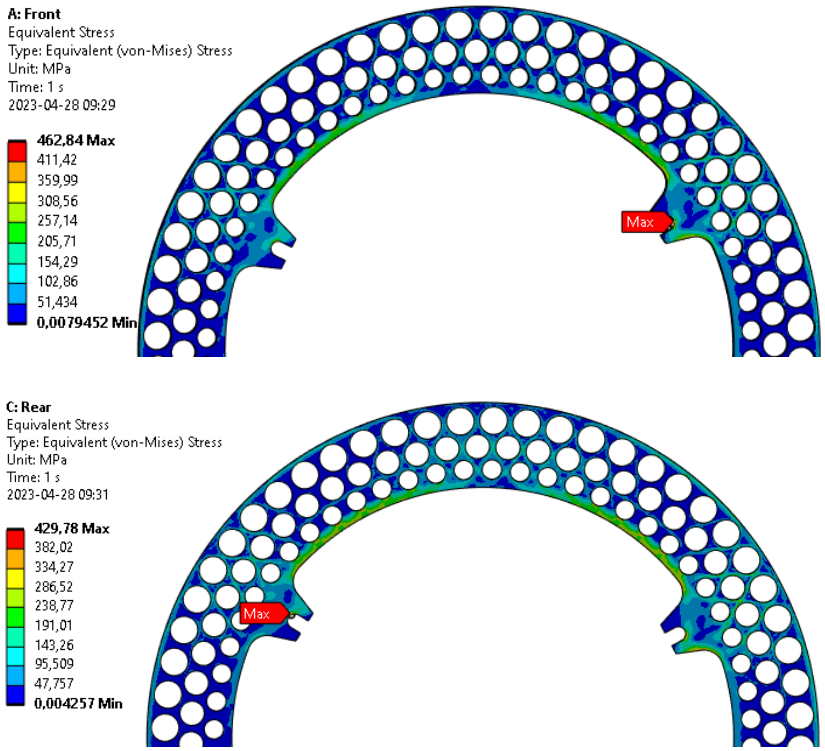

Figure 29: Stress in the front brake disc (top) and rear brake disc (bottom).

In order to compare the new design to the CFS22 design, the carry-over parts were weighed and the mass of the new components was estimated using measurements from CAD models. Table 11 presents all components' masses and their comparison to the CFS22 design. The total weight reduction for the complete brake system was 986 g.

Table 11: Weight of the final concept compared to the CFS22 design.

	Component	CFS22	Final Concept	Comparison (%)
Front	Active caliper side	284 g	284 g	0% (COP)
	Passive caliper side	202 g	66 g	-67%
	Brake pads	128 g	128 g	0% (COP)
	Brake disc	328 g	233 g	-29%
	Mounting parts	111 g	111 g	0% (COP)
	Total:	1 053 g	822 g	-22%
Rear	Active caliper side	121 g	121 g	0% (COP)
	Passive caliper side	90 g	39 g	-57%
	Brake pads	74 g	74 g	0% (COP)
	Brake disc	328 g	117 g	-64%
	Mounting parts	90 g	90 g	0% (COP)
	Total:	703 g	441 g	-37%

5.4 Upright

The design process for the upright and the evaluation of the topology optimization will be presented in this chapter.

5.4.1 Integration of components to the upright

The primary objective was to minimize mass by eliminating any redundant material. As seen in Figure 30, CFS22 used bolted joints for mounting the cooling jacket and gearbox to the upright. By integrating the cooling jacket and inner planet carrier of the gearbox to the upright, early evaluations showed promising results by distributing the load more evenly throughout the part, reducing local stress concentrations, and optimizing the material used.

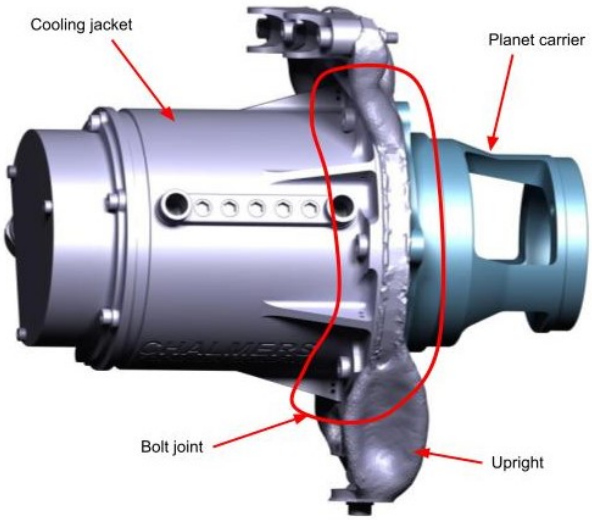

Figure 30: Bolted joint between cooling jacket, upright, and gearbox on the CFS22 wheel assembly.

5.4.2 Design volume

The design volume is a geometric shape that defines the boundaries of where the upright and its integrated parts can occupy space without clashing with other parts in the wheel assembly. The design of the upright takes into consideration the serviceability and accessibility of critical components such as the brake caliper, linkages, and brake disc. To achieve this, the design volumes are carefully planned to ensure that the topology optimization algorithm does not place any material in these areas. This is done by designing toolpaths within the design volume that allow for the mounting of various parts. Since the front and rear upright are different, two separate design volumes were modeled.

5.4.3 Topology optimization of design volume

The front and rear design volumes were transferred to the topology optimization tool along with the previously specified load cases from Tables 3 and 4. The optimization was performed using a coarse mesh of 8 mm due to the project's computational limitations. This provided a rough estimation of where the optimization algorithm removes material and the design volume was refined based on this estimate. This process was repeated several times with decreasing mesh sizes until the design volume was small enough to use a mesh size of 4 mm. Figure 31 shows the topology-optimized solutions of the rear control volume under the same load case but using two different mesh sizes. The optimization algorithm will never leave material thinner than three times the mesh size, which is the minimum thickness required to capture the stress distribution.

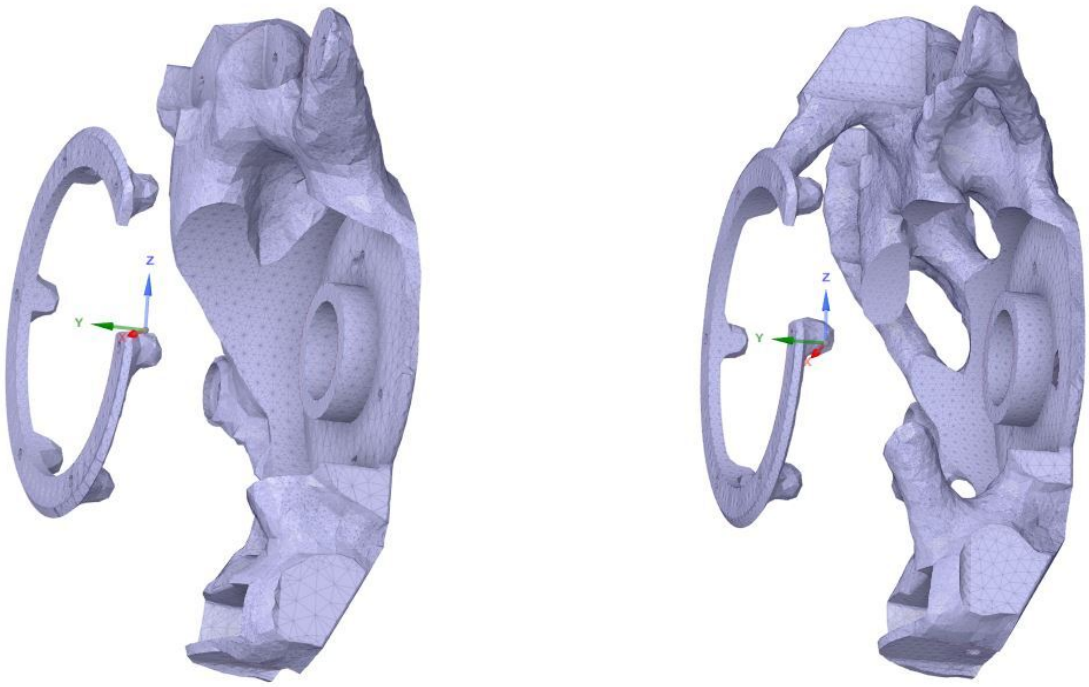

Figure 31: Topology optimization of rear upright with 6 mm mesh size (left) and 4 mm mesh size (right).

5.4.4 Final concept

The final concept of the upright integrates the cooling jacket and the inner planet carrier, see Figure 32. Table 12 shows that the final upright concept, including the new cooling jacket, results in a total weight reduction of 2.6 kg between all four wheel assemblies compared to the CFS22 upright and cooling jacket.

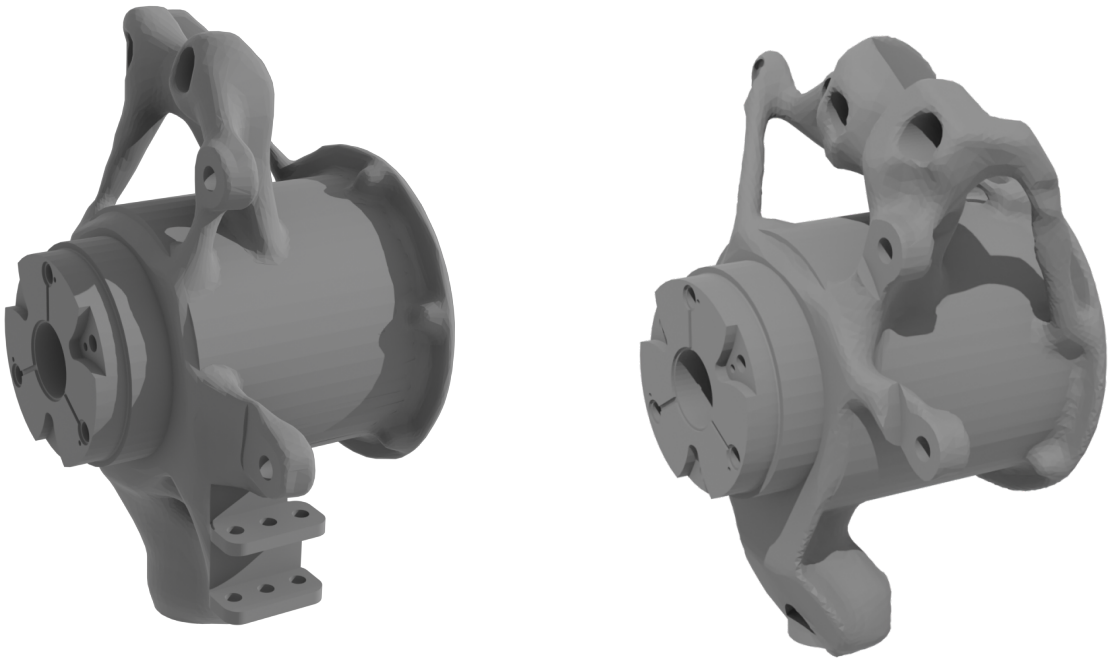

Figure 32: Final concept of the front upright (left) and rear upright (right) integrated with cooling jacket and inner planet carrier.

Table 12: Weight of final concept compared to CFS22 upright and cooling jacket.

Component	**CFS22**	**Final Concept**	**Comparison (%)**
Front	1508 g	793 g	-53%
Rear	1420 g	802 g	-44%
Total:	2928 g	1595 g	-46%

Among many other validations, the upright was simulated for camber and toe compliance to fulfill requirements 1.1 and 1.2, see Figure 33. The results of these simulations are presented in Chapter 6. Due to complications encountered during the simulations, the evaluation of the rear upright was unable to be completed within the set time frame, therefore no camber or toe compliance was evaluated.

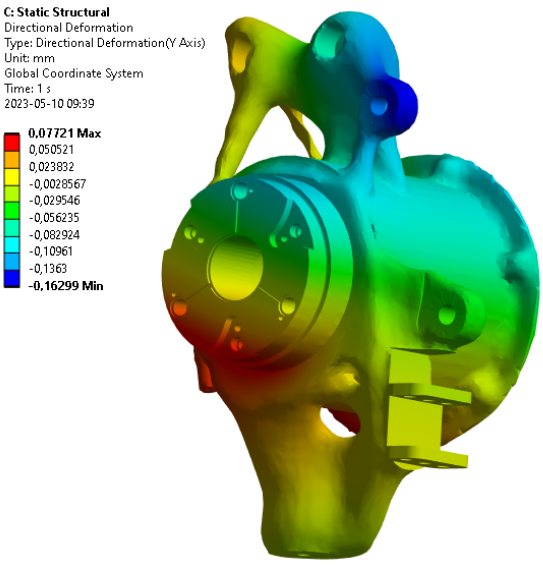

Figure 33: Deformation in the y-direction in the front upright during the worst load case.

For the final simulation of the topology-optimized front upright, the maximum stress was found during the load case Cornering+Bump, from Table 3. The maximum stress was located on the inside edge of the cooling jacket with a stress of 196 MPa, see Figure 34. Since the maximum stress is located in less than one element and the surrounding volume had a stress below 166 MPa, this localized stress can be neglected.

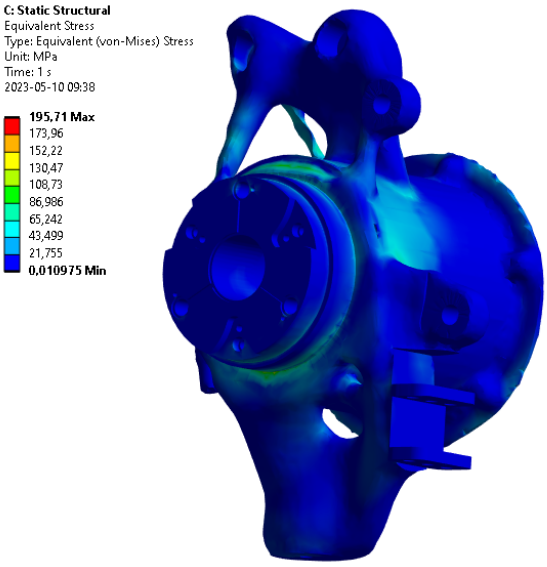

Figure 34: Stress in front upright during the worst load case.

5.5 Final assembly

The final concept combines all the new designs from the sub-systems described in Chapter 5, as illustrated in Figure 35. Since the inner planet carrier and the cooling jacket are integrated into the upright, the total length of the wheel assembly decreased from 192 mm to 154 mm.

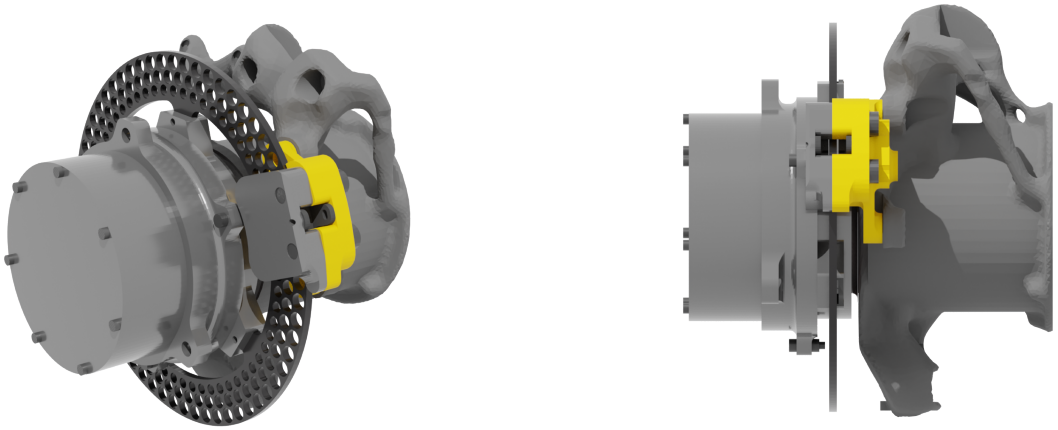

Figure 35: Isometric view (left) and side view (right) of the final rear wheel assembly

The total weight reduction for both the front and rear, with a comparison to the CFS22 design, is presented in Table 13. Summing up the weight reduction for two front wheel assemblies and two rear, results in a combined weight saving of 5.3 kg.

Table 13: Weight of the new concept compared to CFS22.

	Sub-system	**CFS22**	**Final Concept**	**Comparison (%)**
Front	Upright + Cooling jacket	1 508 g	793 g	-53%
	Gearbox	2 673 g	2 261 g	-15%
	Brakes	1 053 g	822 g	-22%
	Total:	5 234 g	3 876 g	-26%
Rear	Upright + Cooling jacket	1 420 g	802 g	-44%
	Gearbox	2 673 g	2 261 g	-15%
	Brakes	703 g	441 g	-37%
	Total:	4 796 g	3 504 g	-27%

The camber and toe compliances had rather strict requirements according to the specification. Due to the limitations in the project's computational power, the full wheel assembly could not be simulated at once. Therefore the total compliance was calculated as the sum of the compliance from the different sub-systems, as seen in Table 14.

Table 14: Compliance in the wheel assemblies.

Front

Component	**Camber**	**Toe**
Gearbox	0.032°	0.008°
Upright	0.029°	0.05°
Linkages	0.01°	0.025°
Rim	0.15°	0.0°
Total:	0.221°	0.083°

Rear

Component	**Camber**	**Toe**
Gearbox	0.016°	0.007°
Upright	Not eval.	Not eval.
Linkages	0.01°	0.025°
Rim	0.15°	0.0°
Total:	Not eval.	Not eval.

The front wheel assembly meets the requirement for compliance in the form of Camber and Toe. Due to the inability to conduct simulations for camber or toe compliance for the rear upright, the rear wheel assembly can not be completely evaluated.

6 Conclusion

The purpose of the project was to improve the CFS22 wheel assembly and create a new weight-optimized design, based on a set of requirements and constraints. This was achieved using a product development methodology, topology optimization, and various softwares.

The final wheel assembly design integrates the cooling jacket and inner planet carrier into the upright, resulting in weight savings and fewer fasteners. Despite the added complexity of post-processing, the benefits outweigh the disadvantages because of the substantial reduction in weight. For future work, it is necessary to further investigate the deformation and maximum stress in the rear upright. The rear upright was not evaluated in this work due to the limitations in computational power. The aim should be to run all simulations on a cluster with more computational power to speed up the design process.

The new cooling jacket presents significant improvements over the CFS22 model. Firstly, it reduces weight and pressure drop whilst staying within the required temperature limits. Secondly, it provides a more uniform temperature distribution, leading to increased motor performance. The design eliminates the need for an inner wall, simplifying the post-processing stage. However, a sealing mechanism is instead necessary to prevent coolant leakage. In the future, software utilizing AI-generated layouts could provide an alternative to manually designed cooling channels.

By splitting the gearbox housing, the size of the inner bearing could be reduced. Splitting the planet carrier allows the outer planet carrier to be machined using 3-axis CNC, and the inner planet carrier to be integrated into the upright. This resulted in fewer parts, and since 3-axis CNC machines are available in-house, it also reduces manufacturing time and cost. The simulated forces exerted by the gears during acceleration are carried over from previous CFS designs, which lack proper documentation. For future work, rigid body dynamics simulations should be used to validate these load cases and if possible, reduce them.

As for the brake system, the new design uses single-acting calipers in both the front and the rear, which reduces the size as well as the weight. The mass of the brake discs was reduced while preserving the braking performance, with the limiting load case being the heat generated during heavy braking. The thermal load case that was used neglects any cooling effects such as convection to the air and is therefore a conservative estimate. By improving this estimation, further mass reduction could be made.

In conclusion, the project successfully achieved its objective of improving the CFS22 wheel assembly and creating a more weight-optimized design. The use of product development methodology assured a structured process for generating and evaluating

various ideas in order to finally select the optimal concept. Then the use of topology optimization resulted in weight savings and more efficient material usage. The new design integrates multiple components, eliminating the need for extra fasteners and simplifying the manufacturing process. Future work includes validating load cases using rigid body dynamics simulations, investigating stress and deformation in the rear upright, and improving thermal load case estimation to reduce further mass for the brake disc. The project provides valuable insights into the design and optimization of wheel assemblies and can be useful for future research in this field.

References

[1] Formula Student Germany, "All known universities and teams," 2023. [Online]. Available: https://www.formulastudent.de/teams/all-universities/ (accessed on: 2023-02-10).

[2] Formula Student Germany, "Rules & documents: Fs-rules 2023 v1.1.pdf," 2023. [Online]. Available: https://www.formulastudent.de/fsg/rules/ (accessed on: 2023-01-20).

[3] Chalmers Formula Student, "Garage," 2023. [Online]. Available: https://www.chalmersformulastudent.se/garage (accessed on: 2023-01-20).

[4] D. Hrovat, "Influence of unsprung weight on vehicle ride quality," *Journal of Sound and Vibration*, vol. 124, no. 3, p. 497, 1988. DOI: 10.1016/S0022-460X(88)81391-9.

[5] S. Hamidizadeh, N. Alatawneh, R. R. Chromik, and D. A. Lowther, "Comparison of different demagnetization models of permanent magnet in machines for electric vehicle application," *IEEE Transactions on Magnetics*, vol. 52, no. 5, pp. 1–4, May 2016. DOI: 10.1109/TMAG.2015.2513067.

[6] M. Andersson, J. Bergström, E. Hanusa, W. Horngacher, I. Kustura, and R. Willner, "Simulering av drivlina samt kylsystem i en elektrisk formula studentbil," Chalmers University of Technology, 2022.

[7] F. M. White, *Fluid Mechanics, Eight Edition in SI Units*. McGraw-Hill Education, 2016, p. 337.

[8] F. P. Incropera, D. P. D. T. L. Bergman, and A. S. Lavine, *Incroperas Principles of Heat and Mass Transfer*. John Wiley Sons Inc, 2017, p. 8.

[9] M. Evertsson, M. Mägi, and K. Melkersson, *Maskinelement*. Studentlitteratur, 2017, p. 485.

[10] H. Wäpling, "Herman wäpling final report cfs22," Chalmers Formula Student, 2022.

[11] Formula Student Austria, "Formula student austria competition handbook 2023 v1.1," 2023. [Online]. Available: https://fsaustria.at/wp-content/uploads/FSA-Competition-Handbook-2023_1-2-1.pdf (accessed on: 2023-01-26).

[12] Formula Student Netherlands, "Formula student netherlands competition handbook 2023 v1.0," 2023. [Online]. Available: https://www.formula-student.nl/wp-content/uploads/2022/12/FSN2023-Competition-Handbook-V1.0.pdf (accessed on: 2023-01-26).

[13] K. Ulrich, S. Eppinger, and M. Yang, *Product design and development, seventh edition*. USA: McGraw-Hill Education, 2020.

[14] M. Tyrbo, private communication, Mar. 2023.

[15] Z. Oulounis, private communication, Mar. 2023.

[16] B. Mehta, private communication, Mar. 2023.

[17] E. Zalnezhad, D. Ahmed, A. A. D. Sahran, M. H. A. Shukor, and B. Asri, "A fuzzy logic based model to predict the fretting fatigue life of aerospace al7075-t6 alloy," *Caspian Journal of Applied Sciences Reasearch*, vol. 1, no. 12, p. 11, 2012.

[18] EOS GmbH, "Eos aluminum alsi10mg - material data sheet," 2022. [Online]. Available: https://www.eos.info/03_system-related-assets/material-related-contents/metal-materials-and-examples/metal-material-datasheet/aluminium/material_datasheet_eos_aluminium-alsi10mg_en_web.pdf (accessed on: 2023-04-18).

[19] K. Bennion, "Electric motor thermal management research," National Renewable Energy Laboratory, 2017. [Online]. Available: https://www.nrel.gov/docs/fy18osti/67121.pdf (accessed on: 2023-03-15).

[20] L. A. Ladino and S. H. Rondon, "Resistance of copper wire as a function of temperature," *Physics Education*, vol. 50, no. 1, p. 42, Dec. 2014. DOI: 10.1088/0031-9120/50/1/42.

[21] H. Cotton, *Basic Electrotechnology*. London: Macmillan Education UK, 1973, pp. 82–93.

[22] P. Wei, Z. Wei, Y. Chen, Y. He, and J. Du, "Thermal behavior in single track during selective laser melting of alsi10mg powder," *Applied Physics A*, vol. 123, no. 604, Aug. 2017. DOI: 10.1007/s00339-017-1194-9.

[23] R. Willner, private communication, Feb. 2023.

[24] J. Chiou, "The effect of nonuniform fluid flow distribution on the thermal performance of solar collector," *Solar Energy*, vol. 29, no. 6, pp. 487–502, 1982. DOI: 10.1016/0038-092X(82)90057-3.

[25] WayKen, "Wall thickness necessary consideration for 3d printing," 2021. [Online]. Available: https://waykenrm.com/blogs/wall-thickness-necessary-%20consideration-for-3d-printing/ (accessed on: 2023-04-23).

[26] H. Wäpling, "Technical starting point," 2023.

[27] SKF, "General rod end specifications," 2023. [Online]. Available: https://www.skf.com/id/products/plain-bearings/spherical-plain-bearings-rod-ends/rod-ends/general-rod-end-specifications (accessed on: 2018-06-28).

[28] Chalmers Formula Student, "Data from endurance run," unpublished.

[29] SKF, *Rullager*. SKF-koncernen, 2019.

[30] P. S. Ghahfarokhi, A. Kallaste, A. Belahcen, and T. Vaimann, "Determination of heat transfer coefficient for the air forced cooling over a flat side of coil," *Electrical, Control and Communication Engineering*, vol. 15, no. 1, p. 1128, 2019. DOI: 10.2478/ecce-2019-0003.

7 Appendix

7.1 Idea generation for the brake system

Brake calipers

Table 15: A table showing all concepts related to the brake caliper.

Brake caliper concept 1	Carry-over and use the same original AP-racing calipers the CFS22 used.
Brake caliper concept 2	Buying a different brand and or model of double-acting caliper.
Brake caliper concept 3	Buying a complete single-acting caliper.
Brake caliper concept 4	Replace the rear side of a double-acting caliper with a custom in-house designed rear side without pistons. Making the caliper single-acting.
Brake caliper concept 5	Integrating the caliper into the upright. The brake caliper would be a permanent part of the upright and would have to be manufactured in the same way as the upright.

Brake discs
Position concept 1: Mounting the brake disc on an extended piece of the driveshaft of the motor towards the car.

Position concept 2: Mounting the brake disc between the motor and gearbox inside the upright.

Position concept 3: Mounting the brake disc on the outside of the gearbox housing.

Brake disc design concept 1: Find and purchase a complete brake disc.

Brake disc design concept 2: A in-house designed and manufactured brake disc.

7.2 Appendix B: Morphological matrix

7.2.1 Cooling Jacket

	Layout	Cross section	Spacing	Pros	Cons
1	Helix	Constant	Constant	• Simple to design	• Increased axial temperature gradient
2	Helix	Constant	Decreasing	• Reduced axial temperature gradient	• Hard to design
3	Helix	Decreasing	Constant	• Reduced axial temperature gradient	• Hard to design
4	Helix	Decreasing	Decreasing	• Reduced axial temperature gradient	• Very hard to design
5	Axial	Constant	-	• Simple to design	• Increased axial temperature gradient

6	Axial	Varying	-	• Decreased axial temperature gradient	• Hard to design

7.2.2 Gearbox

	Flip gear	Split carrier	Split Housing	Pros	Cons
1			X		• Unnecessary split • Difficult to post-process the mating surface between gear and carrier
2				• No additional housing flanges	• Difficult to post-process the mating surface between gear and carrier • One large bearing and one smaller

3		X	X	• Manufacturable in 3-axis CNC • Two smaller bearings	• Added complexity from housing split
4		X		• Manufacturable in 3-axis CNC • No additional housing flanges	• One large bearing and one smaller
5	X		X	• Two smaller bearings	• Difficult to post-process the mating surface between gear and carrier • Added complexity from housing split
6	X				• Impossible to assemble without splitting the housing or planet carrier
7	X	X	X	• Manufacturable in 3-axis CNC • Two smaller bearings	• Added complexity from housing split

8	X	X		• Manufacturable in 3-axis CNC • Two smaller bearings • No additional housing flanges	• Housing must be unnecessary large to be able to assemble the gears

7.3 Appendix C: Concepts

7.3.1 Cooling jacket concepts

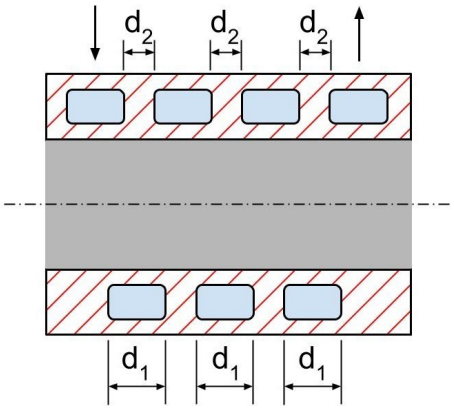

Channel concept 1: Constant channel width and constant channel spacing.

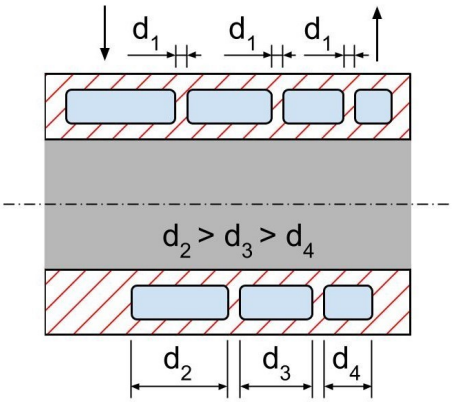

Channel concept 2: Decreasing channel width and constant channel spacing.

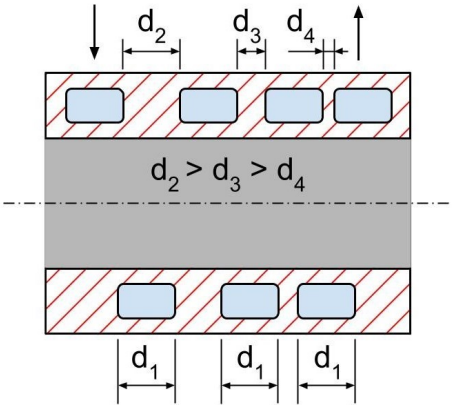

Channel concept 3: Constant channel width and decreasing channel spacing.

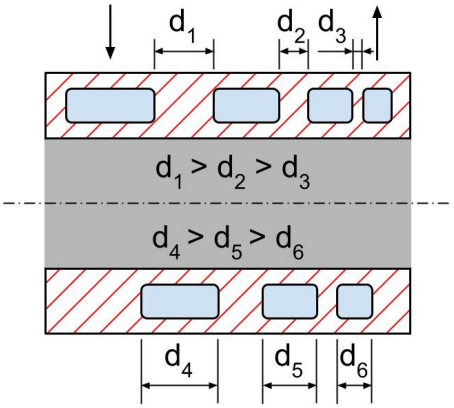

Channel concept 4: Decreasing channel width and decreasing channel spacing.

7.3.2 Gearbox concepts

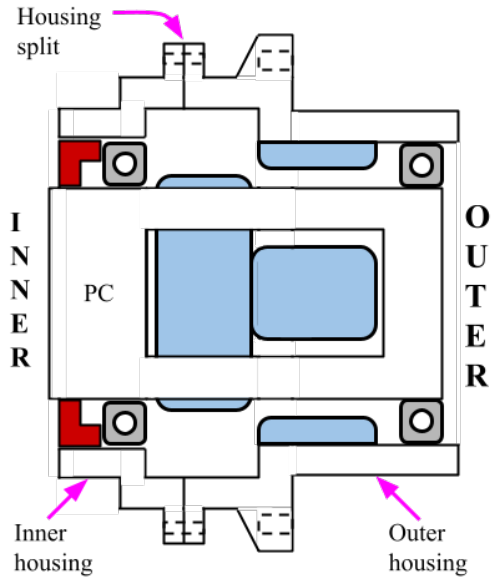

Concept 1: Two-piece housing, no two-piece planet carrier, no flip gears.

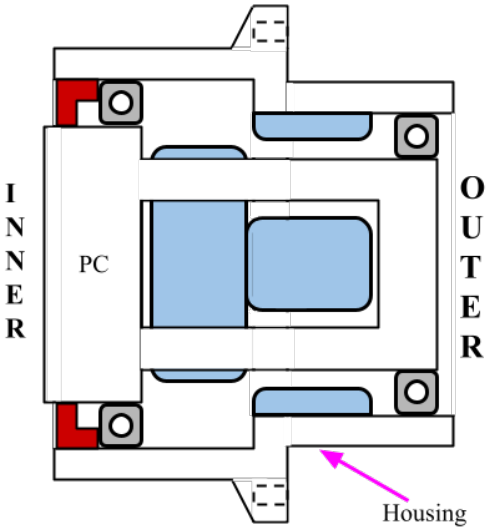

Concept 2: No two-piece housing, no two-piece planet carrier, no flip gears.

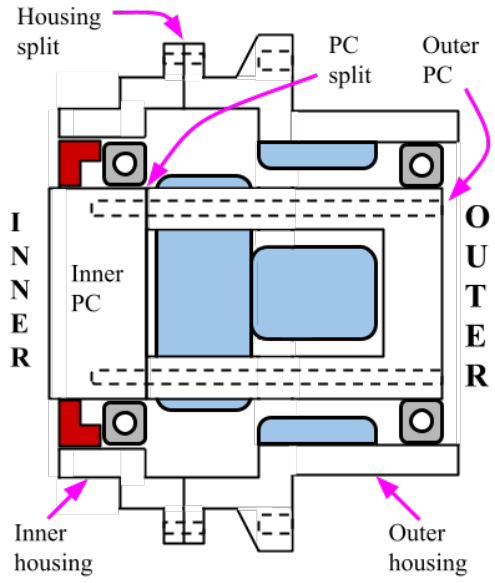

Concept 3: Two-piece housing, two-piece planet carrier, no flip gears.

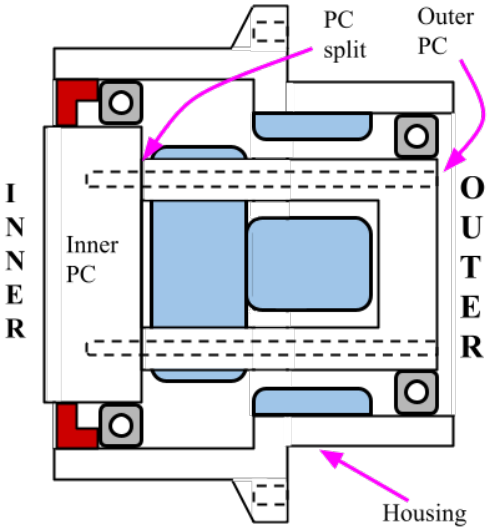

Concept 4: No two-piece housing, two-piece planet carrier, no flip gears.

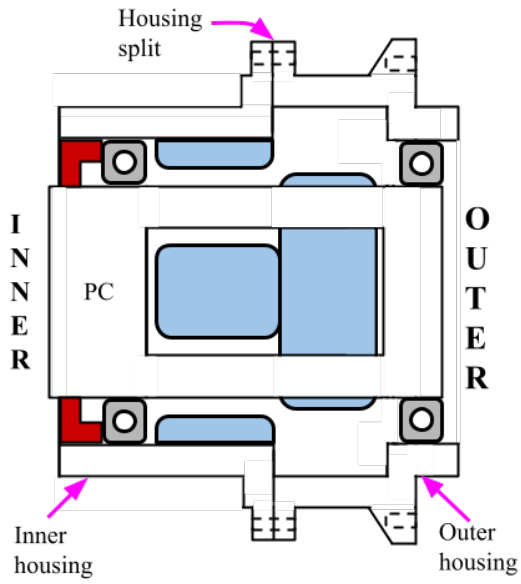

Concept 5: Two-piece housing, no two-piece planet carrier, flip gears.

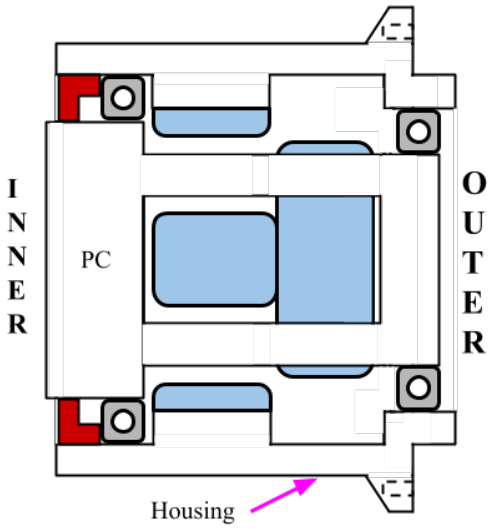

Concept 6: No two-piece housing, no two-piece planet carrier, flip gears.

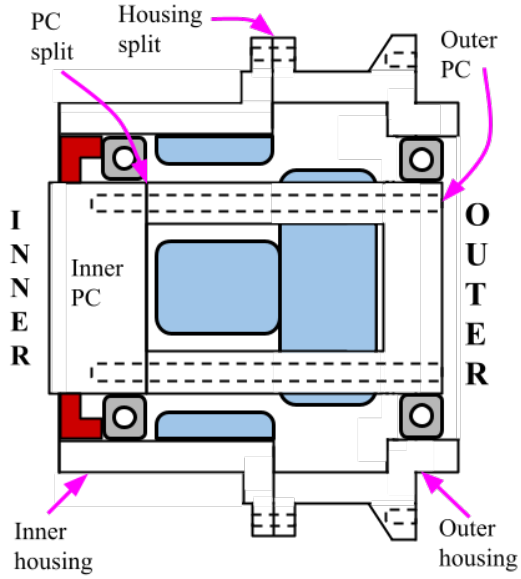

Concept 7: Two-piece housing, two-piece planet carrier, flip gears.

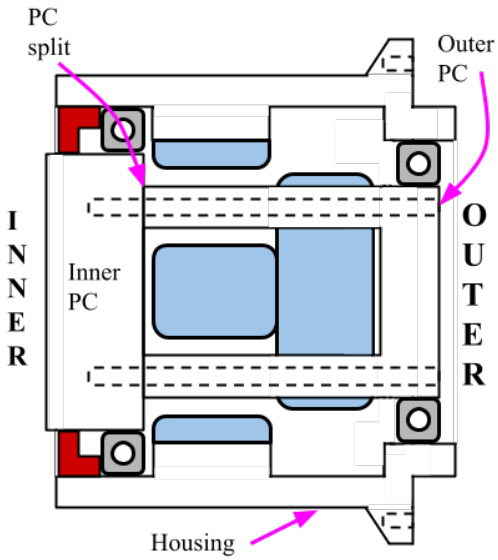

Concept 8: No two-piece housing, two-piece planet carrier, flip gears.

Figure 41: Generated concepts for gearbox

7.4 Appendix D: Calculations

7.4.1 Compliance calcualations

The compliance of the wheel assembly also depends on the compliance of rod ends, and ball joints, used to mount it to the chassis. The rod ends used by CFS are SA8C and SA6C made by SKF which both have an estimated compliance of 8 µm according to their tolerance standard ISO 12240-4 [27]. The linkages have one of these at each end giving each linkage an estimated compliance of 0.016 mm.

In the vertical direction, the linkages are spaced with 180mm which, using trigonometry, gives an added angular compliance of roughly 0.01° in the camber direction. In the forward direction, the linkages are spaced 72 mm which results in an estimated compliance of 0.025° in the toe direction.

7.4.2 Parameters for CFD simulations

Because there is no data for the water temperature when the ambient temperature is at its assumed maximum of $30°C$ it needs to be calculated. From the heat convection formula

$$\dot{Q} = \alpha(T_1 - T_2) \tag{2}$$

where α is the heat transfer coefficient and $\dot{Q}$ is the transferred heat [8], the following relations can be derived for the cooling system:

$$\alpha(T_{water,data} - T_{ambient,data}) = P_{cooling-system} \tag{3}$$

$$\alpha(T_{water,max} - T_{ambient,max}) = P_{cooling-system} \tag{4}$$

Assuming that the power of the cooling system is not depending on the ambient temperature and the same applies to the heat transfer coefficient the following equations can be derived.

$$\alpha(T_{water,data} - T_{ambient,data}) = \alpha(T_{water,max} - T_{ambient,max}) \tag{5}$$

$$\Rightarrow T_{water,max} = T_{water,data} - T_{ambient,data} + T_{ambient,max} \tag{6}$$

Inserting $T_{water,data} = 47.5°C$ and $T_{ambient,data} = 18°C$ recorded from an endurance run [28] and assuming a maximum ambient temperature of $30°C$ Equation 6 gives $T_{water,max} = 59.5°C$.

7.4.3 M4 Grade 8.8 bolts (Housing)

Equations regarding the bolts holding the two housing parts together. Due to the geometry of the housing the bolts will not be subject to any axial forces (Nothing greater than the pretension). Therefore the equations consider the required bolt pretension to

avoid slipping when braking and the worst case if the bolts are only in shear without pretension.

Calculations for M4 bolts without pretension.

$$F_{tot,tang} = \frac{M_{brake}}{r} = \frac{350}{0.068} = 5147N \tag{7}$$

$$F_{tang} = \frac{F_{tot,tang}}{n_{bolts}} = \frac{5147}{3} = 1716N/bolt \tag{8}$$

$$A_{bolt} = \frac{\pi \cdot d_{min}^2}{4} = 8.25 \cdot 10^{-6} m^2 \tag{9}$$

$$\sigma_{max,shear} = \frac{F_{tang}}{A_{bolt}} = 208MPa \tag{10}$$

$$Safety\ factor\ (Shear) = \frac{800 \cdot 0.8 \cdot factor}{\sigma_{max,shear}} = 1.85 \tag{11}$$

Calculations for M4 bolts with pretension.

$$F_{tot,ax} = \frac{M_{brake}}{r \cdot \mu} = \frac{350}{0.068 \cdot 0.7} = 7353N \tag{12}$$

$$F_{ax} = \frac{F_{tot,ax}}{n_{bolts}} = \frac{7353}{3} = 2451N/bolt \tag{13}$$

$$\sigma_{max,ax} = \frac{F_{ax}}{A_{bolt}} = 297MPa \tag{14}$$

$$Saftey\ factor\ (Tensile) = \frac{800 \cdot 0.8}{\sigma} = 2.16 \tag{15}$$

The first calculation confirms that even in the worst case when the bolts are only experiencing shear stress they will be sufficient. The second calculation confirms that the bolts will be able to handle the required preload so the two housing parts will not slip when braking.

7.4.4 M5 Grade 8.8 bolts (Planet carrier)

Based on the load cases presented in Chapter 4.3, it can be seen that the forces acting on the front and rear wheels are distinct. As the highest forces are present in the rear wheel assembly, the dimension force is determined as the force applied to the rear wheel assembly. All the equations presented in this chapter come from Chapter [9].

A conservative assumption was made, that all the load is applied to the planet carrier top. Realistically the load is applied to the wheel which then is transferred to the housing and follows into the bearings. Bearings are both attached to the planet carrier's inner and outer, meaning the load will be distributed between the parts.

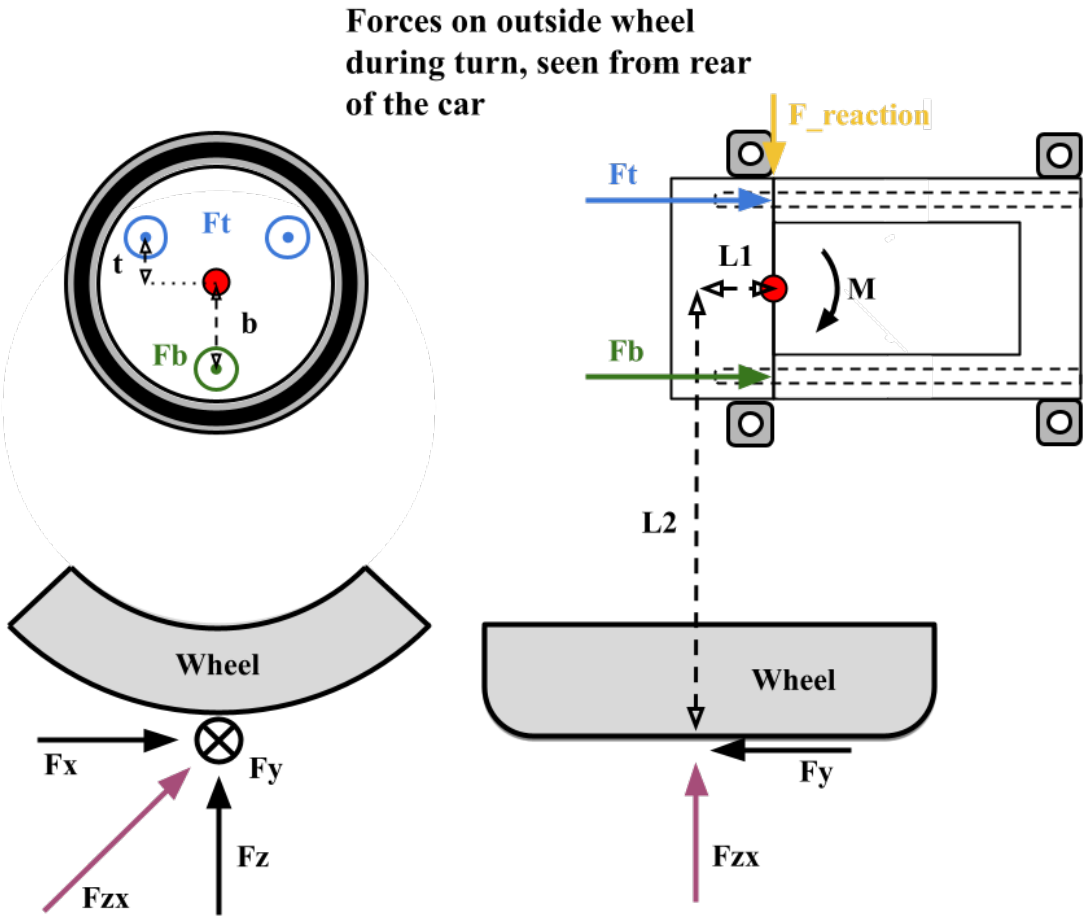

Figure 42: Force equilibrium for front right wheel.

A force equilibrium, Figure 42, was set up to calculate the outer force for both the front right and rear right wheel assembly during left hand turn. One side of the planet carrier will in compression and the other side will be in tension. The bolt force, F_s, is the dimension factor and therefore the compression force, F_k, will not be considered. Cause of the weight transfer during turning the inside tires will be subjected to significantly less force than the outside tires. It is assumed that the outside tire force will be the dimensional factor. To determine the bolt force and minimum preload the equations below were used:

$$c_s = \frac{E_{bolt} \cdot A_{bolt}}{L} \tag{16}$$

$$c_k = \frac{E_{PC} \cdot A_{PC}}{L} \tag{17}$$

$$F_{0,front} = \frac{c_k \cdot F_N}{c_k + c_s} = 5691\ N \tag{18}$$

$$F_{0,rear} = \frac{c_k \cdot F_N}{c_k + c_s} = 5700\ N \tag{19}$$

$$F_{s,front} = F_0 + \frac{c_s \cdot F_N}{c_k + c_s} = 7516\ N \tag{20}$$

$$F_{s,rear} = F_0 + \frac{c_s \cdot F_N}{c_k + c_s} = 7529\ N \tag{21}$$

The smallest force needed for preload will be 5691 N for the front planet carrier and 5700 N for the rear planet carrier to not get play. The maximum tensile force the bolts will experience is 7516 N in the front planet carrier and 7529 N in the rear planet carrier. This is less than the force required to break the threads in the 3D-Printed part, which was validated during the tensile test, see Appendix 7.5.

To determine the largest stress amplitude in the bolts the following equations was used:

$$A_{sp} = \frac{\pi}{16} \cdot (d_1 + d_2)^2 \tag{22}$$

$$\sigma_{s,max} = \frac{F_N}{A_{sp}} \tag{23}$$

$$\sigma_{s,min} = \frac{F_0}{A_{sp}} \tag{24}$$

$$\sigma_{a,front} = \frac{\sigma_{s,max} - \sigma_{s,min}}{2} = 34.9\ MPa \tag{25}$$

$$\sigma_{a,rear} = \frac{\sigma_{s,max} - \sigma_{s,min}}{2} = 35.3\ MPa \tag{26}$$

The maximum stress amplitude, 35.3 MPa, will be in the rear planet carrier when the applied preload was 6500 N. A bolt of grade 8.8 has a maximum stress amplitude of 50-60 MPa, the conclusion is that the M5 bolt will be able to meet the requirements.

7.4.5 Bearing life cycle analysis

The life cycle calculations were made in MATLAB with SKF Bearing analysis theory [29]. The total life cycle for the bearing complex in the gearbox is calculated to be 1220 million rotations. The car is estimated to travel a maximum distance of 3000 km resulting in 2.3 million revolutions. Since this is significantly less than the calculated value, the bearings in the gearbox will be sufficient.

7.5 Appendix E: Tensile test

Holes that are threaded in aluminium use helicoils to prevent wear and increase thread strength. This will be used for the M5 bolts that hold the planet carrier to the upright. The goal with the test is to see how much force can be applied before failure. Using a tensile test machine, Figure 43a, two tests were preformed for 6mm and 10mm M5 helicoils.

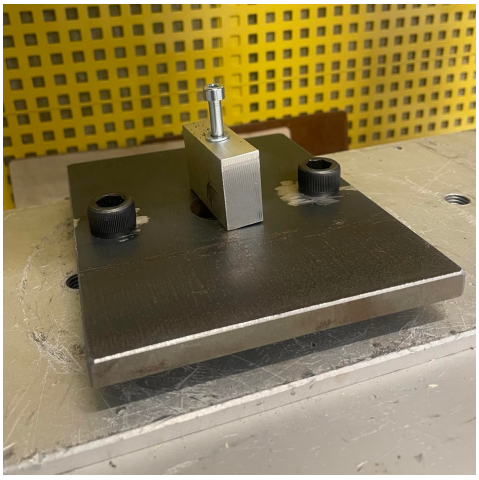

(a) Setup showing how the tensile test was carried out.

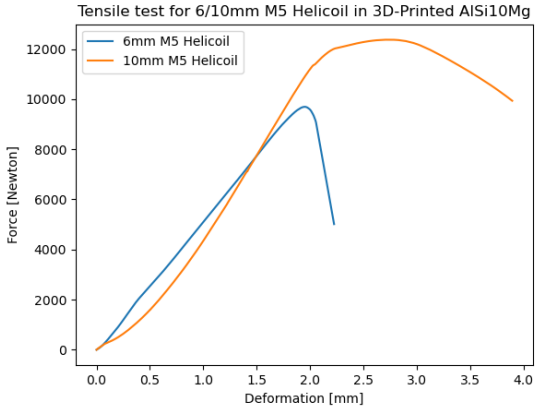

(b) Tensile test plot showing force vs elongation.

Figure 43: Stress and deformation in the gearbox during 60° tilt test.

Results are displayed in a graph, Figure 43b, plotting force vs elongation. Ultimate failure for each length helicoil was as follows:

- M5 6mm Helicoil: 9694 N (Threads in AlSi10Mg failed)
- M5 10mm Helicoil: 12 486 N (Bolt failed)

7.6 Appendix F: Cooling jacket

7.6.1 Parameters for the cooling jacket concept

Starting with the evaluation of the number of turns, Table 18 shows that to achieve a low pressure drop it is beneficial to have a low number of turns. On the other hand, doing so increases the temperature on the inner wall which is consistent with the theory presented in Chapter 1.1.

Table 18: Data from simulations of different numbers of turns.

Number of turns	$T_{max,innerwall}(°C)$	$\Delta P(kPa)$
2	78.51	0.82
3	75.19	1.43
4	73.16	2.50

When having a design with 2 turns the channels get wide, see Figure 44a, which makes it prone to smaller defects affecting the flow. That could mean that the flow gets uneven, which leads to higher temperatures. Wider channels also lower the Reynolds number which makes more parts of the flow not strictly turbulent and laminar, which has a negative effect on the heat transfer and thus on the temperature. This effect is noticeably smaller when instead having 3 turns, see Figure 44b, and even less when having 4 Turns, see Figure 44c. It is also simpler to even out the temperature difference over the cooling jacket when having a design with more turns. A design with 3 turns was viewed as the best compromise between a low pressure drop, low wall temperature, and channel width because it is the design with the lowest number of turns that still has reasonably narrow and controllable channels.

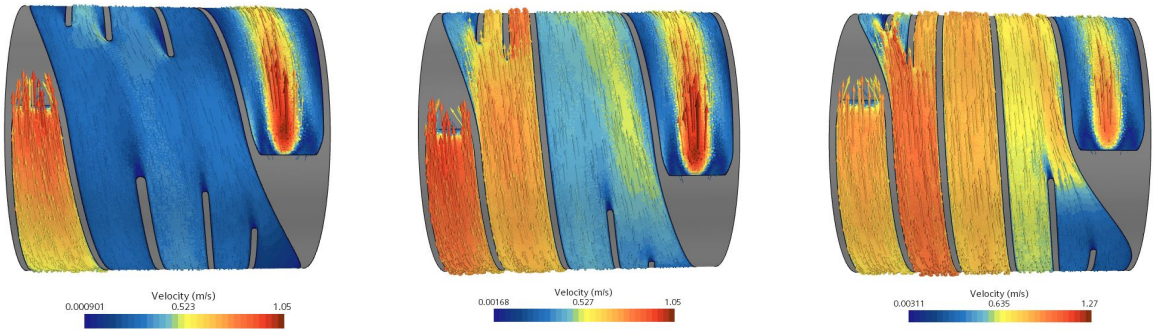

(a) 2 Turns. **(b)** 3 Turns. **(c)** 4 Turns.

Figure 44: Different number of helix turns with the velocity distribution visualized.

Table 19 shows data from simulations with the previous concept choices but with different radial channel thicknesses. A channel thickness of 2 mm gave a pressure drop

higher than the requirements specification demands and was therefore not considered. Having a thickness of 3 mm resulted in a pressure drop of about 29% lower than the CFS22 design, whereas 4 mm thick channels give a 54% lower pressure drop than the CFS22 design. The drawback with thicker channels is that the mass and the maximum temperature increases. The thickness of 3 mm was considered to have a big enough reduction in pressure drop compared to the CFS22 design and because the overall aim of the project is to reduce the weight it was considered to be better than the 4 mm option and was therefore chosen.

Table 19: Data from simulation of different number of turns.

Height (mm)	$\boldsymbol{\Delta P(kPa)}$	**Mass incl. water (g)**	$\boldsymbol{T_{max,innerwall}(°C)}$
2	3.40	233	72.81
3	1.43	273	75.33
4	0.93	312	77.58

The pitch of the chosen Channel concept 4 has a linear profile. Different gradient constants were simulated to find the one that gives the best temperature distribution and hence the lowest maximum temperature on the inner wall. Table 20 shows that a gradient constant of approximately 4 achieves this.

Table 20: Data from simulation of different number of turns.

k	$\boldsymbol{T_{max,innerwall}(°C)}$
0	74.69
2	74.39
4	74.14
6	74.54
8	74.95

7.6.2 Cooling jacket no inner wall and inner wall comparison

Having no inner wall was compared to having an inner wall by simulating both versions with equal channel and port layouts. On the design with no inner wall, a thin inner wall was added to be able to apply the heat from the motor and simulate the motor's outer wall's ability to spread the heat. This meant that the main difference between the two concepts from a simulation standpoint was the difference in the diameter of the cooling channels.

Table 21: Data from simulation of having an inner wall or not.

Concept	$\boldsymbol{T_{max,innerwall}(°C)}$	$\boldsymbol{\Delta P(kPa)}$
Inner wall	74.48	1.62
No inner wall	74.90	1.48

Table 21 shows that having an inner wall slightly reduces the maximum temperature on the inner wall towards the motor but at the cost of having a slightly higher pressure drop. This is expected because having an inner wall makes the diameter of the channels larger, hence resulting in longer channels. Long channels are beneficial for lowering the temperature, but at the same time increase the pressure drop. Because the differences between the versions were considered small, and both had advantages and disadvantages compared to each other, their overall cooling performance was considered to be equal.

7.6.3 Cooling jacket convection with ambient air

When simulating convection with the external air, an ambient temperature of $30°C$ was used. Due to the aerodynamics of the car, the airspeed at the cooling jacket is close to $0m/s$ even when driving at higher speeds [6]. According to [30] the heat transfer coefficient α for air that is not moving is about $5W/(m^2K)$. Table 22 shows that the difference between having no convection and convection with $\alpha = 5W/(m^2K)$ results in a difference of $0.03°C$. This value was considered to be small enough to be neglected.

Table 22: Data from simulations with and without convection with the ambient air.

$\boldsymbol{\alpha(W/(m^2K))}$	$\boldsymbol{T_{ambient}(°C)}$	$\boldsymbol{T_{max,innerwall}(°C)}$
0 (No convection)	30	75.19
5	30	75.16

7.7 Appendix G: Simulations Gearbox

60° Tilt test

In competitions, a tilt test of 60° is conducted to see if anything is leaking [2]. To ensure the gearbox can hold the forces from a tilt test a simulation was performed and the maximum stress was 44 MPa with a maximum deformation of 0.035 mm. Stresses can be seen in Figure 45a and deformations can be seen in Figure 45b:

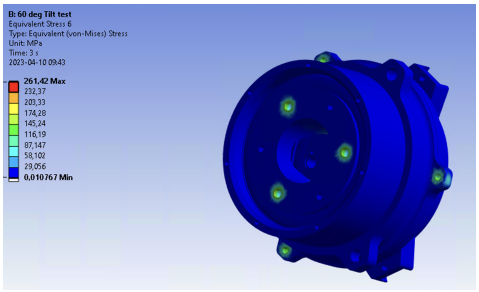

(a) Stresses in gearbox during 60° tilt test.

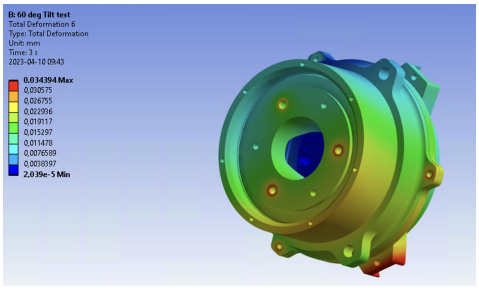

(b) Deformation in gearbox during 60° tilt test.

Figure 45: Stress and deformation in the gearbox during 60° tilt test.

Braking

During braking, both stress (90 MPa) and deformation (0.064 mm) is below the acceptable limit, see Figure 46. The three M4 bolts clamping the two housing pieces together will be sufficient according to the hand calculations in Appendix 7.4.3.

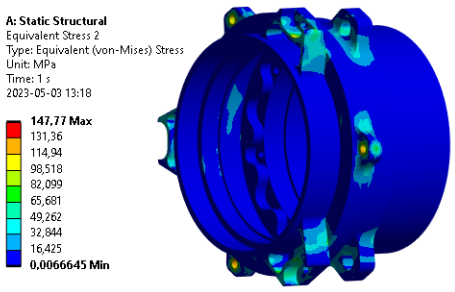

(a) Stress in gearbox housing during braking.

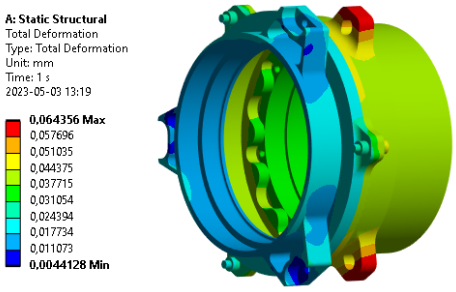

(b) Deformation in gearbox housing during braking.

Figure 46: Stress and deformation in gearbox housing during braking.

Acceleration Planet carrier

Figure 47a shows the equivalent stresses on the outer planet carrier (7075-T6) and inner planet carrier (AlSi10Mg). The forces are a result of the motor torque which is later transferred into the gearset. Since the outer planet carrier is keyed into the inner planet carrier the stresses in the bolts will not be evaluated in this FEM simulation. The maximum stress in these components is 170 MPa respectively 120 MPa, which ensures a factor of safety of 2, see Figure 47a.

Maximum deformation occurs in the outer planet carrier, Figure 47b, with a magnitude of 0.166 mm. Currently, the deformation in the center of the pinshaft is 0.135 mm and should be less than 0.1 mm according to CFS22. Due to uncertainty in the magnitude of the applied forces, further investigation should be performed to verify if any redesign is necessary.

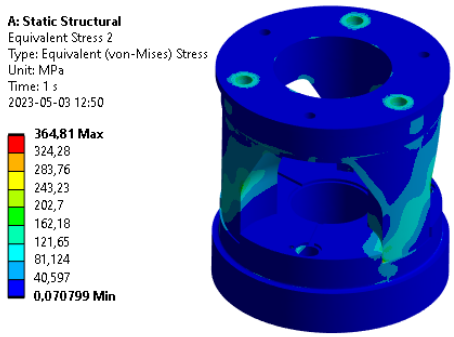

(a) Stress in planet carrier during acceleration.

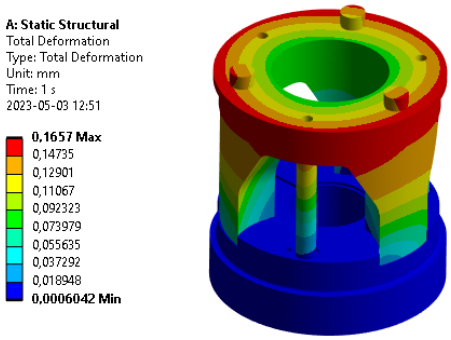

(b) Deformation in planet carrier during acceleration.

Figure 47: Stress and deformation in planet carrier during acceleration.

Acceleration Housing

When the motor applies maximum torque to the gearset the highest stress in the housing is 100 MPa with a deformation of 0.020 mm, see Figure 48. Forces are applied to the inside of the housing where the ring gear mounts while holding the rim fixed.

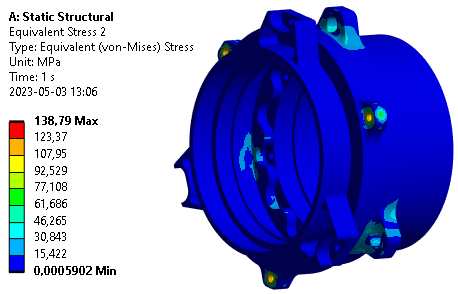

(a) Stress in gearbox housing during acceleration.

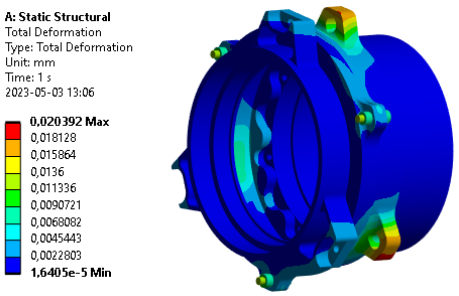

(b) Deformation in gearbox housing during acceleration.

Figure 48: Stress and deformation in gearbox housing acceleration.

7.8 Appendix H: Simulations Brake system

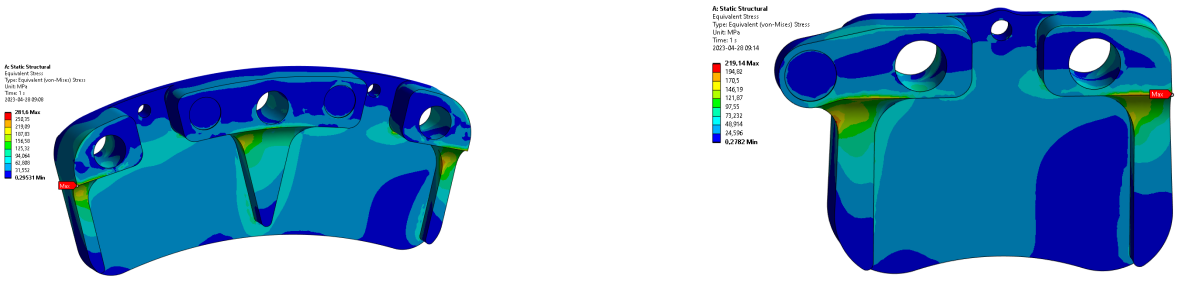

Figure 49: Resulting stress for the front (left) and rear (right) caliper passive side.

Table 23: Maximum deformation and stress for front caliper rear side.

Front caliper	Result	Max allowed
Deformation	0.32 mm	0.35 mm
Stress	281.6 MPa	286 MPa

Table 24: Maximum deformation and stress for rear caliper rear side.

Rear caliper	Result	Max allowed
Deformation	0.25 mm	0.35 mm
Stress	219.1 MPa	286 MPa

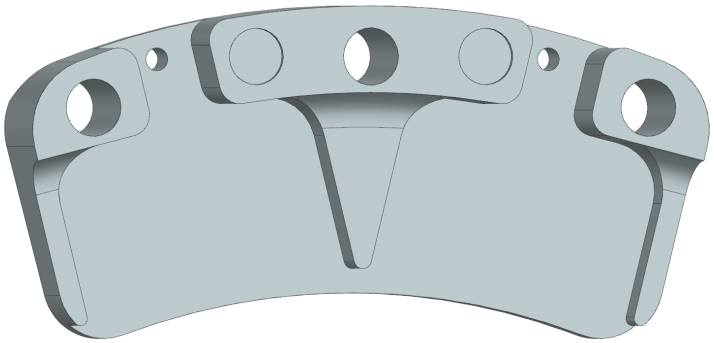

Figure 50: Front caliper custom designed passive side.

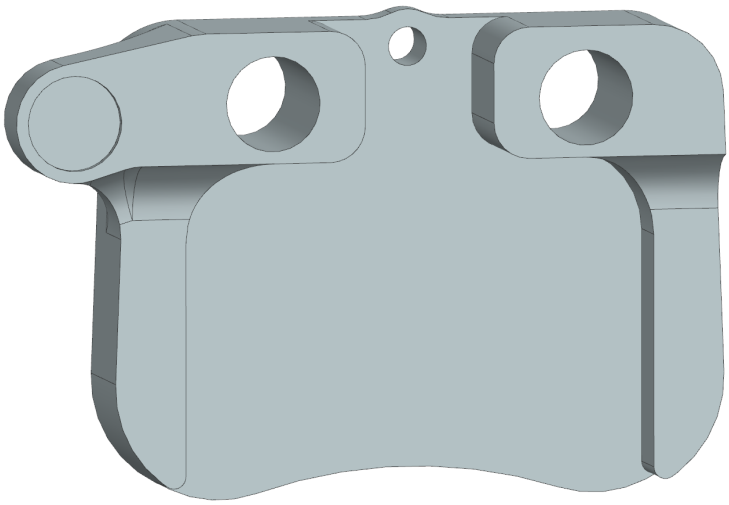

Figure 51: Rear caliper custom designed passive side.

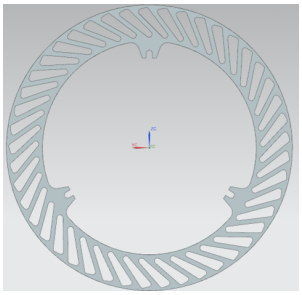

(a) Disc design 1.

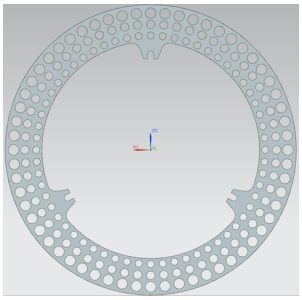

(b) Disc design 2.

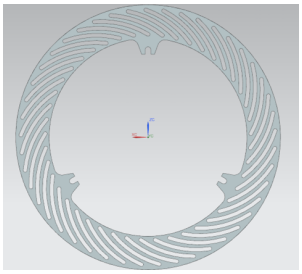

(c) Disc design 3.

Figure 52: Disc designs.

(a) Front disc displacement.

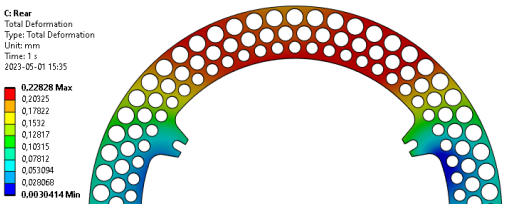

(b) Rear disc stress.

Figure 53: Rear disc displacement.

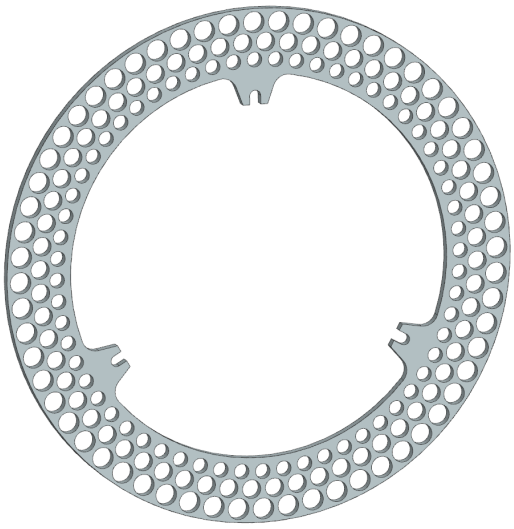

Figure 54: Custom designed brake disc.

Table 25: Maximum deformation and stress for front and rear brake discs.

Brake discs	**Front**	**Rear**
deformation	0.20 mm	0.23 mm
Stress	463 MPa	430 MPa